



Article

Precision Lost with Complexity: On an Extraordinary New Species of Pholcidae (Araneae, Smeringopinae) from Western DR Congo [†]

Arnaud Henrard *D, Rudy Jocqué *, Nathalie Smitz D and Virginie Grignet

Royal Museum for Central Africa (RMCA), Leuvensesteenweg 13, 3080 Tervuren, Belgium; nathalie.smitz@africamuseum.be (N.S.); virginie.grignet@africamuseum.be (V.G.)

- * Correspondence: arnaud.henrard@africamuseum.be (A.H.); rudy.jocque@africamuseum.be (R.J.)
- [†] ZooBank: urn:lsid:zoobank.org:pub:C067F995-86E2-40F0-A824-8B0C2D7330CB; urn:lsid:zoobank.org:act:84506CA8-AD88-43A3-BAD2-E637DAC52FB6.

Abstract

A remarkable new pholcid spider species is described from the Democratic Republic of the Congo: *Smeringopina polychila* sp. nov. The male is distinguished by a unique and previously undocumented structure, here termed the "parachila", which has not been observed in any other spider to date. The description is complemented by high-quality illustrations, including detailed drawings, photographs, micro-CT scans, and 3D reconstructions of the genitalia and the newly discovered male structure. Remarkable intraspecific variations, both somatic and genitalic, in males are also highlighted and discussed. A phylogenetic analysis based on the cytochrome *c* oxidase subunit I, 16S ribosomal RNA and histone H3 gene fragments is presented to tentatively place the new species into an existing phylogenetic framework. The results of the molecular analyses confirm that the new species belongs to the subfamily Smeringopinae and is nested within the genus *Smeringopina* Kraus, 1957.

Keywords: Africa; intraspecific variations; new taxa; phylogeny; micro-CT; Smeringopina



Academic Editor: Peter Michalik

Received: 19 August 2025 Revised: 22 September 2025 Accepted: 29 September 2025 Published: 15 October 2025

Citation: Henrard, A.; Jocqué, R.; Smitz, N.; Grignet, V. Precision Lost with Complexity: On an Extraordinary New Species of Pholcidae (Araneae, Smeringopinae) from Western DR Congo. *Taxonomy* **2025**, *5*, 57. https://doi.org/10.3390/taxonomy5040057

Copyright: © 2025 by the authors. Licensee MDPI, Basel, Switzerland. This article is an open access article distributed under the terms and conditions of the Creative Commons Attribution (CC BY) license (https://creativecommons.org/licenses/by/4.0/).

1. Introduction

Pholcidae Koch, 1850 are commonly known as cellar spiders or daddy long-legs spiders. With 97 genera and 2047 species currently described, this spider family ranks among the most diverse spider groups worldwide, placing 8th in terms of species richness [1]. Pholcids are primarily tropical, web-weaving spiders that inhabit a wide range of microhabitats [2], including ground-level environments (such as leaf litter or under logs and stones), sheltered spaces (e.g., caves, rock crevices, tree buttresses, and human dwellings), as well as vegetation, particularly the undersides of live leaves. Pholcids are among the most spectacular spiders regarding sexual dimorphism. Males, in particular, may be provided with extraordinarily modified palps and often exhibit remarkable secondary sexual traits, including cheliceral and carapace excrescences (e.g., [3–13]).

A collection of spiders from the Mai Ndombe Province, a poorly inventoried part of Democratic Republic of the Congo, contains a species that rivals even the most remarkable pholcids described to date. Considering the extraordinary morphology of the species, we initially considered establishing a new, albeit monospecific, genus. However, recent studies demonstrated that the taxonomy of spiders and particularly that of Pholcidae, requires molecular data to achieve robust systematic conclusions [14–18]. Our

results in this context revealed that, notwithstanding its unique morphology, the species we here describe falls within a well-established genus. This case also provides an ideal opportunity to test the potential of micro-computed tomography (micro-CT or μ CT) for enhancing the documentation of male palpal structures and the internal morphology of the female genitalia.

2. Materials and Methods

2.1. Collection and Depository

The seven specimens examined during this study were collected during the "2021 Expedition BINCO RD-CONGO" organized in collaboration with Biodiversity Inventory for Conservation (BINCO) organization (see [19]). All biological samples collected on this expedition are labelled with the code BINCO_RDC_21_0001, which is a standardized format allowing easy tracking of where the material is deposited, who identified it, and what was used in publications. Types and other specimens examined are deposited in the collections of the Royal Museum for Central Africa (RMCA) located in Tervuren, Belgium. The arachnological collection of the RMCA is identified by the acronym "BE_RMCA_ARA.Ara". This acronym is followed by a unique code for each recorded sample, and, for the sake of clarity, it is simplified by RMCA_xxxxxxx in the text.

2.2. Description, Imaging and Illustrations

The specimens, preserved in 70% ethanol, were observed, drawn, and measured with a WILD M 10 stereomicroscope. Photographs of the habitus, details of mouthparts, detached male palps, female genitalia, and measurements were taken with a DFC500 camera mounted on a Leica MZ16A and piloted with the LAS automontage software (ver. 4.13). The epigyne was dissected and digested using half a tablet of Total Care Enzima product (protein removal system originally for cleaning contact lenses and containing subtilisin A-0.4 mg per tablet; Abbott Medical Optics, Santa Ana, CA, USA) in a few milliliters of distilled water for several hours or overnight, then immersed back in 70% ethanol to be photographed.

For the micro-computed tomography (μ CT) analyses, a male body, a palp, and the female epigyne were stained with a 1% LUGOL iodine solution for 42 h. After washing in a few milliliters of pure acetone, the samples were air-dried for 24 h, gently fixed with a piece of tape on a carbon stick and then scanned with an XRE-UniTOM (Tescan XRE, Ghent, Belgium) piloted with Aquila software (version 2727, build af20fc9e4ea4) in microfocus mode, with 2000 projections and at 70 keV tube voltage for each scan. The scanning parameters for each body part were as follows: male body (4.8 µm voxel size, 5 W power, 500 ms exposure); male carapaces (2.5–3 μm, 3 W, 550–1000 ms); male palps (1.3 μm, 2 W, 500 ms); and female genitalia (1.5 μm, 2 W, 500 ms). After being scanned, the samples were rehydrated using the Wetting Agent Trisodium Phosphate with Agepon, as described in [20,21]. The acquisition data were first processed using the Panthera 1.2.2. for reconstruction (and image rendering), followed by segmentation and mesh generation in the 3D analysis software Dragonfly 2022 (Object Research Systems (ORS), Montreal, QC, Canada, https://www. theobjects.com/dragonfly/index.html (acessed on 1 February 2022)). The model was further processed in GOM Inspect (https://www.gom.com). Final 3D model, μCT scans, and further photographs of the specimens are visible on the RMCA Virtual Collection website (https://virtualcol.africamuseum.be (acessed on 1 September 2022)).

The map was created with the online tool SimpleMappr [22]. All illustrations were assembled and edited in Photoshop CS5 (white balance and level adjusted, sharpness improved). All palp illustrations are from left palps, except for the male paratype, for which the right palp was taken, and images were reversed to make them appear as if they

Taxonomy **2025**, 5, 57 3 of 28

are the left palp. Terminology of genitalic features and description format follow [15]. All measurements in the text are in mm.

2.3. Abbreviations

ALE—anterior lateral eyes; AME—anterior median eyes; AEP—anterior epigynal plate; asl—above sea level; BL—bulbal lobe (prolateral); BH—bulbus hump; BL—prolateral bulbus lobe; Bu—bulbus; CAE—carapace antero-lateral extension; Che—chelicera; Chi—chilum; CP—bulbus cap-like plate; DLP—dorsal lobe of bulbus prong: DP—distal prong of bulbus; En—endite; Fe—femur; GB—granulated bulge; HS—epigynal internal hornlike structures; Pa—patella; Pch—parachilum; PG—prolateral groove of palp; PLE—posterior lateral eyes; PME—posterior median eyes; PEP—posterior epigynal plate; PP—prolateral process of palpal femur; Pr—procursus; RG—retrolateral groove of palp; RP—retro-basal process of palpal femur; SI—sternum anterolateral incision; Ta—tarsus; Ti—tibia; To1–6—the different tooth-like appendages of bulbus; VLP—ventral lobe of bulbus prong; VP—ventral process of palpal femur.

2.4. Molecular Analyses

2.4.1. DNA Extraction, Amplification, Sequencing and Curation

One and three legs of two specimens, one female and one subadult male (RMCA_247639 and RMCA_247640, respectively), were isolated and further processed for molecular investigation. Individual genomic DNA was extracted using the QIAamp DNA Micro kit (Qiagen, Hilden, Germany) following the manufacturer's instructions, including a digestion time of 4 h and a DNA elution in 50 μL of AE buffer.

Amplifications and sequencings were performed using primers listed in Appendix A.1, Table A1 [23–25]. For 16S and H3 gene fragments, all amplifications were performed in a 20 μ L reaction mixture containing 2 μ L of DNA template, 2 μ L of 10× buffer, 1.5 mM MgCl₂, 0.2 mM dNTP, 0.4 μ M of each primer, and 0.03 units/ μ L of PlatinumTM Taq DNA Polymerase (InvitrogenTM, Waltham, MA, USA). For COI, amplification was carried out in a 12 μ L reaction volume containing 2 μ L of DNA template, 5 μ L of QIAGEN Multiplex (Qiagen, Hilden, Germany), 3.8 μ L of ultrapure water and 0.6 μ L of each primer diluted at 10 μ M. For each DNA region, PCR profile was as displayed in Appendix A.2, Table A2. PCR products and negative controls were checked on a 1.5% agarose gel, using a UV transilluminator and the MidoriGreenTM Direct (NIPPON Genetics Europe, Dueren, Germany) method. Positive amplifications were subsequently purified using the ExoSAP-ITTM protocol (following manufacturer's instructions) and sequenced in both directions by Macrogen Europe (Amsterdam, The Netherlands).

Raw sequences were trimmed, corrected, translated into amino acids and assembled using Geneious Prime[®] 2019.2.3 (Biomatters Ltd., Auckland, New Zealand). A consensus sequence was generated for each specimen and each gene fragment and was then compared against sequences in online reference databases using the BLAST tool in Geneious Prime[®] 2019.2.3 (investigating the database available in the online repository GenBank) and BOLD system v4 [26]. The sequences obtained from the two paratype specimens are deposited in GenBank (see Appendix A.3, Table A3 for accession numbers).

2.4.2. Phylogenetic Analyses

Based on preliminary morphological examination and the blast results, sequences from Smeringopinae taxa were retrieved from GenBank and a combined phylogenetic analysis was performed to tentatively place the new species into an existing phylogenetic framework, (mainly established by [2,14]). The used sequences from GenBank (12S, 16S, 18S, 28S, CO1, H3) originate from different studies [2,14,27–30] and accession numbers are provided in Appendix A.3, Table A3.

Taxonomy **2025**, 5, 57 4 of 28

Three different datasets were constructed to test the placement of the new species. Dataset 1 (70 terminals, 61 taxa, 2565 sites analysed) includes GenBank DNA sequences from taxa for which at least two above-listed DNA fragments are available. Dataset 2 (46 terminals, 40 taxa, 2565 sites analysed) comprises taxa with at least four DNA fragments (including the newly described species despite its lower marker count). Since the monophyly of Smeringopinae and its position as sister to Pholcinae is robustly established [14,26,27,31], *Spermophora minotaura* Berland, 1920 (Pholcinae) was arbitrarily chosen, based on the availability of its complete gene data, to root trees in analyses of Datasets 1 and 2. The Dataset 3 (34 terminals, 33 taxa, 2708 sites analysed) focuses on *Smeringopina* Kraus, 1957 only (regardless of the number of available genes), and *Smeringopus lesserti* Kraus, 1957 and *S. lotzi* Huber, 2012 were used as outgroups (based on the availability of complete gene data). A few chimera taxa were constructed and included in the analyses (following [2], see Appendix A.3, Table A3).

For each DNA fragment, sequences were aligned with MAFFT v.7 implemented online [32] with default settings. Uncertain positions were removed from alignments using the least stringent settings in Gblocks 0.91b [33,34] performed online at Phylogeny.fr (available online at http://phylogeny.lirmm.fr/phylo_cgi/index.cgi (accessed on 8 May 2025); [35,36]). Combined alignments were then created with Mesquite v3.81 [37] by concatenating the MAFFT–Gblocks curated marker alignments.

To account for the differences in evolutionary dynamics among sites and genes, protein coding genes (COI and H3) were partitioned into single codon positions. For all three datasets, optimal partition schemes and substitution models were evaluated using PartitionFinder 2 [38]. The analysis was performed with PhyML 3.0 [39], using the greedy algorithm [40], setting 'branchlengths' to 'linked' and models choice based on the Bayesian Information Criterion (BIC), evaluating all models of evolution implemented in MrBayes.

Phylogenetic reconstructions were run using statistical approaches including maximum likelihood (ML) and Bayesian inference (BI), and using the model specified by PartitionFinder for each partition. ML analyses were conducted in GARLI v2.1 (Genetic Algorithm for Rapid Likelihood Inference; [41]). To obtain the ML topology with the best likelihood score, 10 search replicates were ran with the following default setting values changed: streefname = random, attachmentspertaxon = [two times the number of taxa], genthreshfortopoterm = 100,000; scorethreshforterm = 0.001 and significanttopochange = 0.0001. Node supports were assessed from 1000 bootstraps obtained with four independent runs of 250 different searches, each starting from a random tree. The following settings were further adjusted to speed up the bootstrapping (cf. GARLI manual): genthreshfortopoterm = 10,000; significanttopochange = 0.01 and treerejectionthreshold = 20. The discrete gamma distribution of rates across sites was set to 6 categories when applicable. The bootstrap values were then summarized on the best ML tree using SumTree 4.0.0 (part of the DendroPy 4.0.0 package, [42]). BI were run using MrBayes v3.2.2 [43–45]. Analyses were conducted between 10,000,000 to 50,000,000 generations, until it was checked that the standard deviation of split frequencies decreased below 0.01 and the tree search was conducted according to MrBayes defaults (two independent runs each consisting of one cold and three heated MCMC chains). Parameters were estimated independently for each partition using the following command: unlink statefreq = (all) revmat = (all) shape = (all) pinvar = (all) tratio = (all). The discrete gamma distribution of rates across sites was set to 6 categories when applicable. Convergence diagnostics were also checked with Tracer V1.7 [46] by examining the effective sample size values (ESS > 200) and to ensure that the Markov chains had reached stationarity. Trees were sampled every 1000th generation and were used to reconstruct a 50% majority rule consensus tree after having discarded the first 25% as burn-in (MrBayes default).

Taxonomy **2025**, *5*, *5*7 5 of 28

Trees were first displayed and drawn in FigTree v1.4.3 [47] then exported in a vector image format (.svg) and edited in Inkscape v. 1.3.2 for final publication.

3. Results

3.1. Molecular Identification and Phylogeny

Fragments of the mitochondrial COI (966 bp), 16S (426 bp) and nuclear H3 (328 bp) DNA genes were scored in two specimens (RMCA_247639 and RMCA_247640). For both specimens, COI, 16S and H3 sequences had identical nucleotide compositions. BLAST searches in GenBank and BOLD system (for COI only) indicated an affinity with *Smeringopina* spp.

Our phylogenetic results are largely congruent with previous studies [14,30]. Analyses recovered two primary clades corresponding to the Northern and Southern groups (Figures 1 and 2), and strong support is found for the two-group monophyly in Dataset 2 analysis (Figure 2). However, relationships both between and within these clades remained unresolved, especially in Dataset 1 analysis (Figure 1).

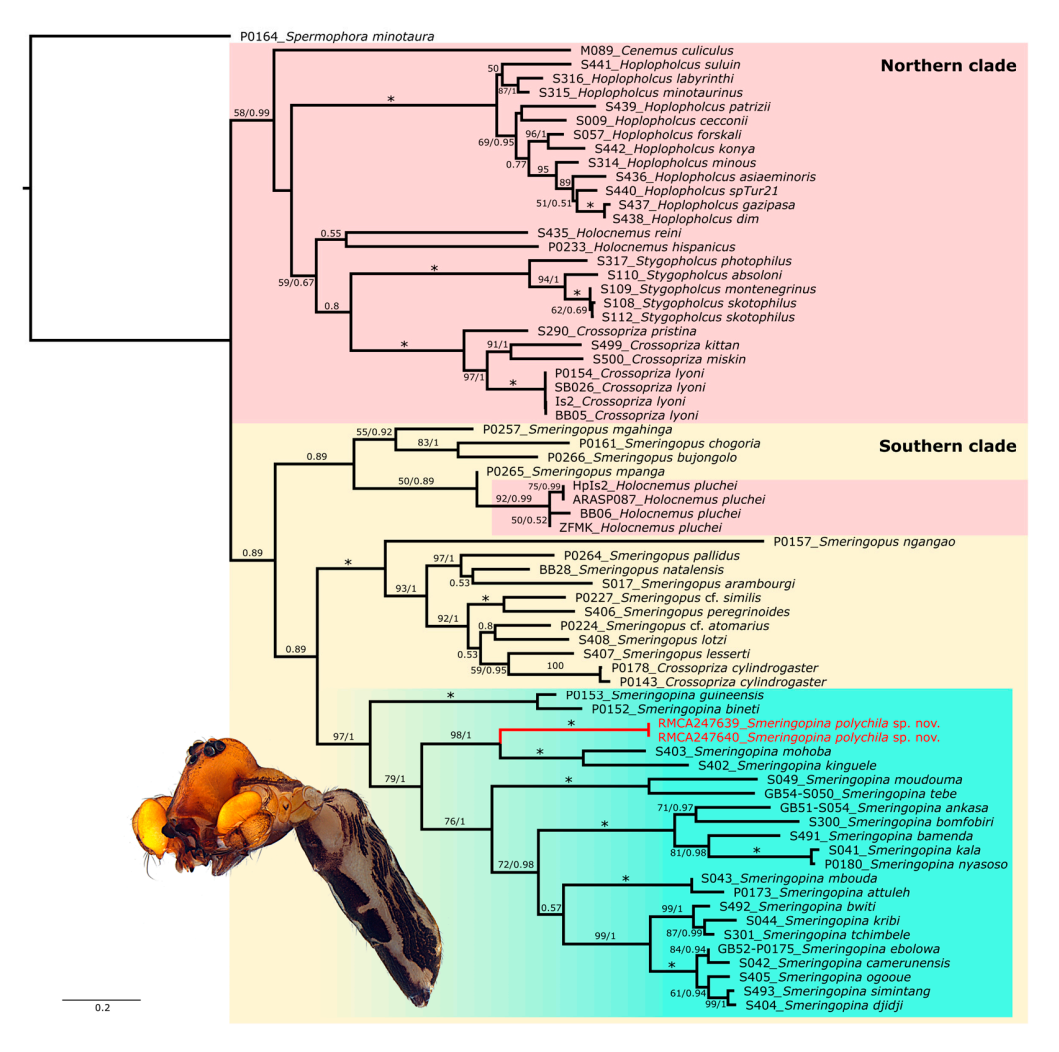


Figure 1. Phylogenetic reconstruction of Smeringopinae based on Dataset 1. Support values (bootstraps and posterior probabilities) from the different analyses run on the combined alignment are shown at branches here on the best ML tree as follows: ML/MB. Values below 0.5/50 are not shown and stars indicate absolute support in both MB and ML analyses. The genus *Smeringopina*, in which the new species *S. polychila* sp. nov. (in red) falls, is highlighted in blue. The photo represents the male paratype (RMCA_247642).

Taxonomy 2025, 5, 57 6 of 28

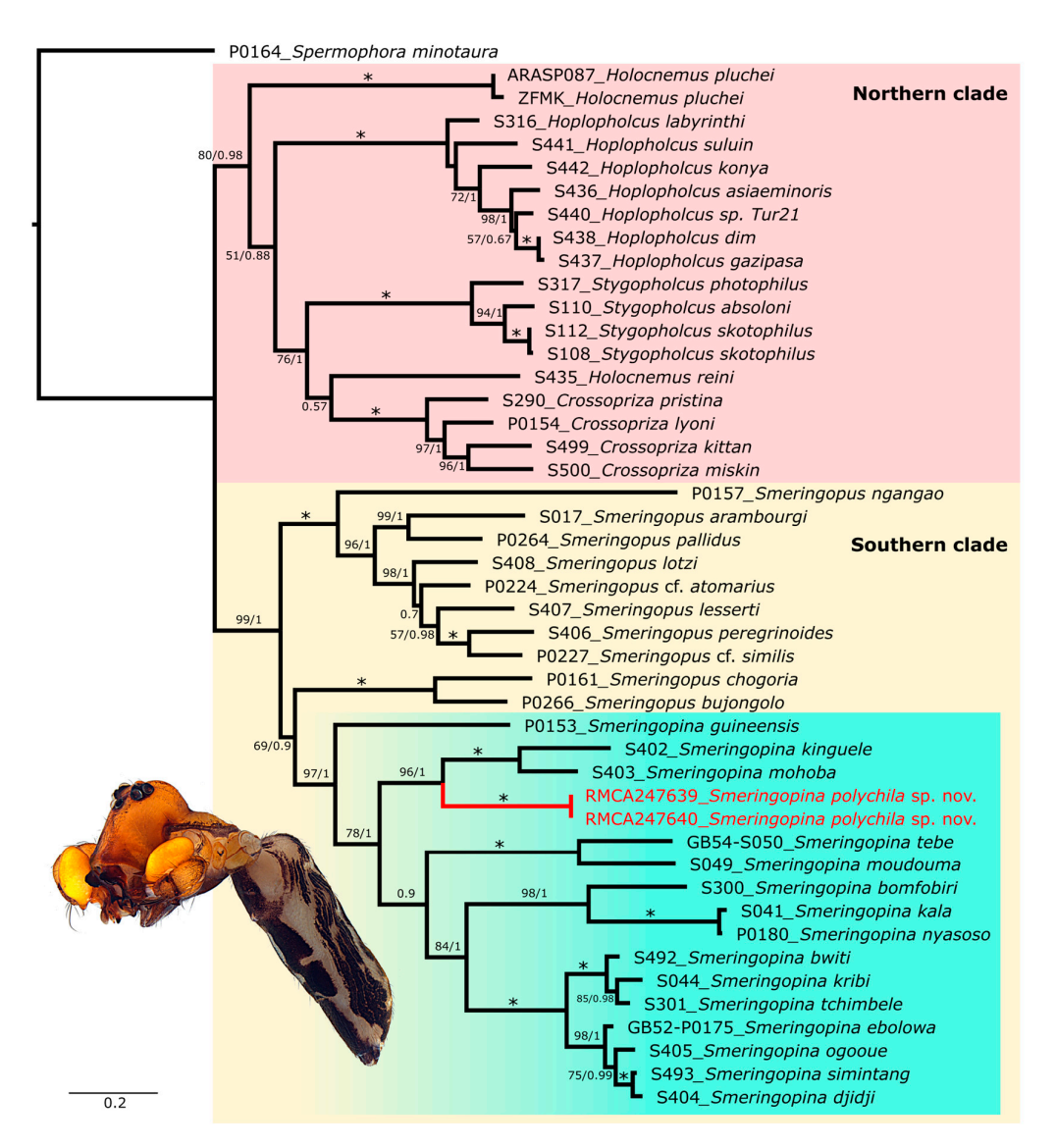


Figure 2. Phylogenetic reconstruction of Smeringopinae based on Dataset 2. Support values (bootstraps and posterior probabilities) from the different analyses run on the combined alignment are shown at branches here on the best ML tree as follows: ML/MB. Values below 0.5/50 are not shown and stars indicate absolute support in both MB and ML analyses. The genus *Smeringopina*, in which the new species *S. polychila* sp. nov. (in red) falls, is highlighted in blue. The photo represents the male paratype (RMCA_247642).

Monophyly of *Crossopriza* Simon, 1893, *Hoplopholcus* Kulczyński, 1908, *Smeringopina*, and *Stygopholcus* was strongly supported in all analyses. *Smeringopus* Simon, 1890 was recovered as paraphyletic in both dataset analyses (Figures 1 and 2), consistent with earlier findings [14,27]. In both analyses, *Holocnemus* Simon, 1873 was not recovered, and *H. pluchei* (Scopoli, 1763) is even nested within *Smeringopus* in Dataset 1 analysis (Figure 1). This unstable phylogenetic position is also reflected in recent studies which tend to demonstrate the non-monophyly of *Holocnemus* as currently defined [14,16,27,30]. Resolving the phylogeny of this group will likely require denser taxon sampling and genomic data analysis.

Within *Smeringopina*, our topology converges with the findings of [14]. Relationships among species and species groups (sensu [8]) were well-resolved in Datasets 1 and 2 (Figures 1 and 2) but poorly resolved in Dataset 3 analysis. Notably, the *guineensis* group did not appear sister to remaining *Smeringopina* in Dataset 3, in contrast to results from Datasets 1 and 2 [14].

Taxonomy 2025, 5, 57 7 of 28

Across all analyses (Figures 1–3), the new species formed a clade sister to a group comprising *Smeringopina kinguele* Huber, 2013, *S. mohoba* Huber, 2013, and *S. fang* Huber, 2013 (traditionally assigned to the *lekoni* group, see [8]). However, like in Huber et al. [14], the *lekoni* group appeared paraphyletic in all analyses.

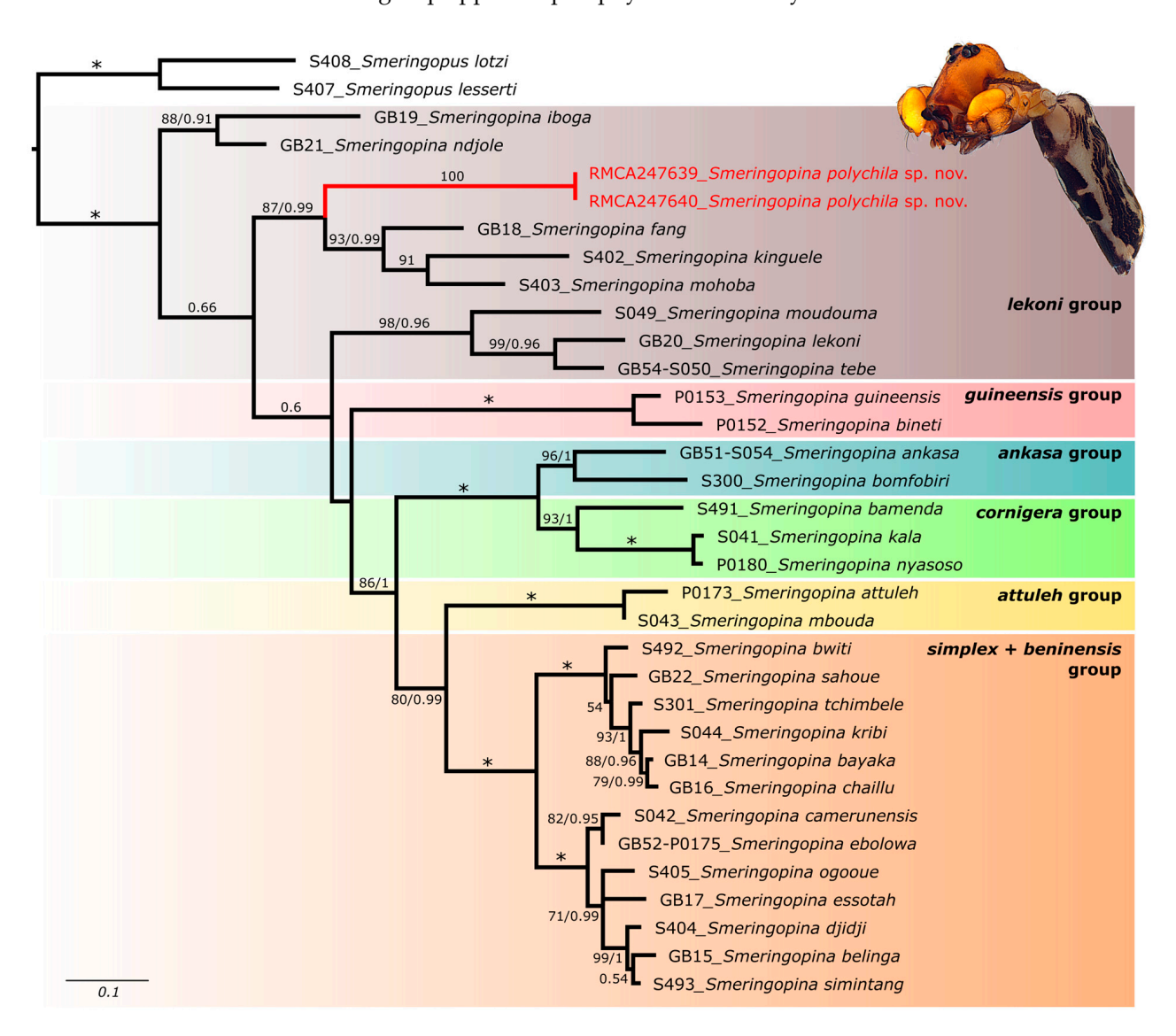


Figure 3. Phylogenetic reconstruction of *Smeringopina* based on Dataset 3. Support values (bootstraps and posterior probabilities) from the different analyses run on the combined alignment are shown at branches here on the best ML tree as follows: ML/MB. Values below 0.5/50 are not shown and stars indicate absolute support in both MB and ML analyses. The different species are highlighted as defined by Huber [8] and Huber et al. [14]. The new species, *S. polychila*, sp. nov., is marked in red. The photo represents the male paratype (RMCA_247642).

3.2. Taxonomy

Class Arachnida Cuvier, 1812

Order Araneae Clerck, 1757

Family Pholcidae C. L. Koch, 1850

Subfamily Smeringopinae Simon, 1893

Genus Smeringopina Kraus, 1957

Smeringopina polychila sp. nov. Henrard & Jocqué

Figures 1, 2, 3, 4A–E, 5A–F, 6A–E, 7A–F, 8A–F, 9A–F, 10A–F, 11A–F, 12A–F, 13A–F, 14A–I, 15A–E and 16.

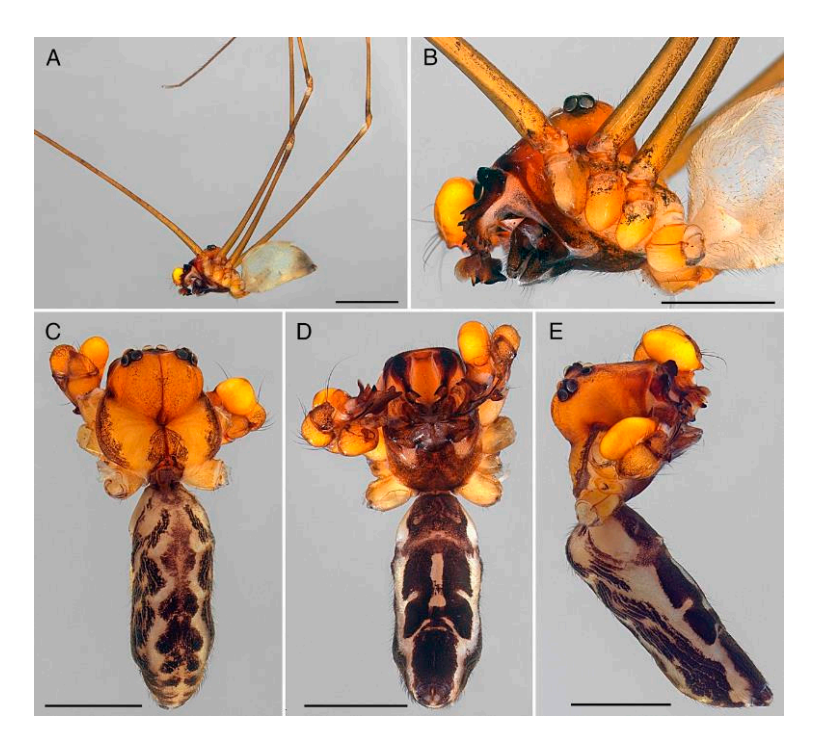


Figure 4. *Smeringopina polychila* sp. nov., males habitus. (**A**,**B**) Male holotype. (**C**–**E**) Male paratype (RMCA_247642). (**A**) Habitus, lateral view. (**B**) Carapace, lateral view. (**C**) Habitus, dorsal view. (**D**) Idem, ventral view. (**E**) Idem, lateral view. Scale bars: (**A**) = 2 mm; (**B**–**E**) = 1 mm.

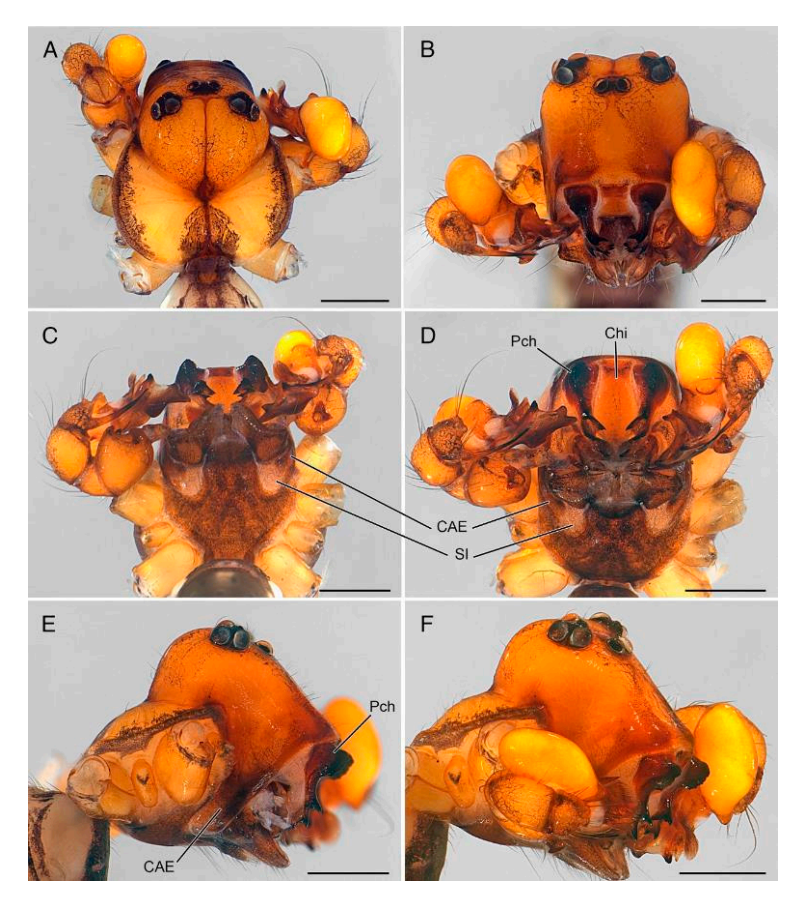


Figure 5. *Smeringopina polychila* sp. nov., male paratype (RMCA_247642). (**A**) Carapace, dorsal view. (**B**) Idem, frontal view. (**C**) Idem, ventral view. (**D**) Idem, ventro-anterior view. (**E**) Idem, lateral view. (**F**) Idem, lateral, slightly oblique view. Abbreviations: CAE = antero-lateral extension of carapace; Chi = chilum; Pch = parachilum; SI = sternum anterolateral incision. Scale bars = 0.5 mm.

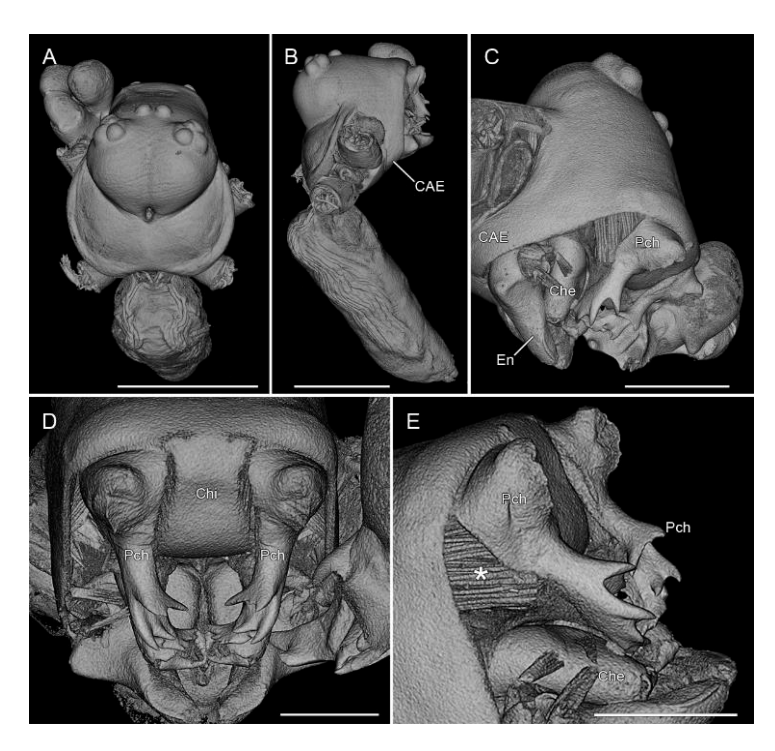


Figure 6. *Smeringopina polychila* sp. nov., μ CT scans of male paratype (RMCA_247642). (**A**) Habitus, dorsal view. (**B**) Idem, lateral view. (**C**) Carapace, lateral, slightly ventral view. (**D**) Idem, detail on the parachila, frontal view. (**E**) Idem, lateral view. The star indicates the muscular fibers connected to the parachilum. Abbreviations: CAE = antero-lateral extension of carapace; Che = chelicera; Chi = chilum; En = endite; Pch = parachilum; SI = sternum anterolateral incision. Scale bars: (**A**–**D**) = 1 mm; (**E**) = 0.5 mm.

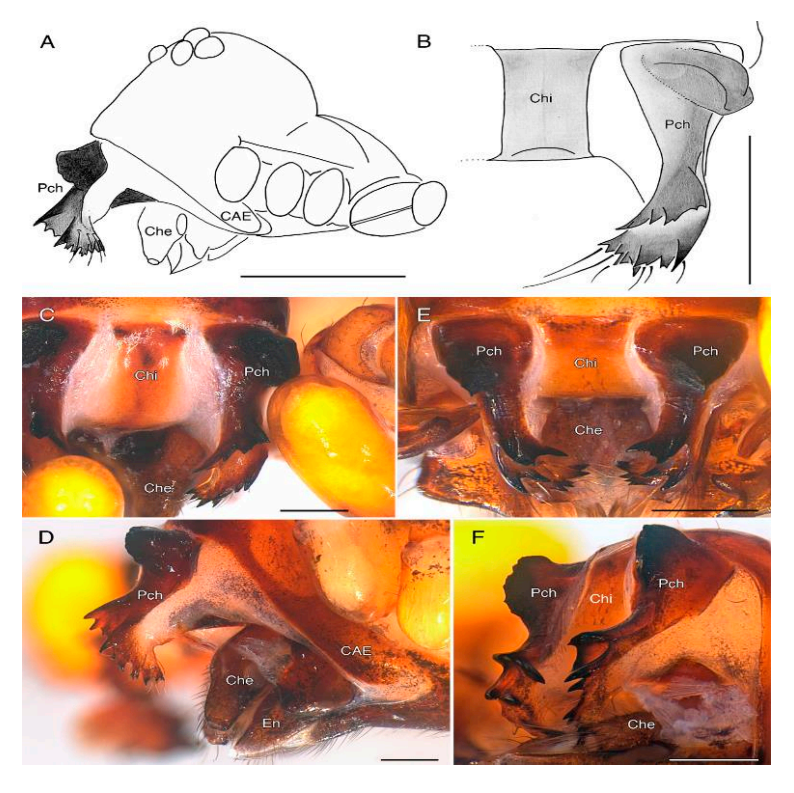


Figure 7. *Smeringopina polychila* sp. nov., male. (**A–D**) Male holotype. (**E,F**) Male paratype (RMCA_247642). (**A**) Carapace, lateral view. (**B,C,E**) Parachila, dorsal view. (**D**) Idem, lateral view. (**F**) Idem, lateral, slightly *oblique* view (mirrored). Abbreviations: CAE = antero-lateral extension of carapace; Che = chelicera; Chi = chilum; En = endite; Pch = parachilum. Scale bars: A = 1 mm; B = 0.5 mm; C - F = 0.2 mm.

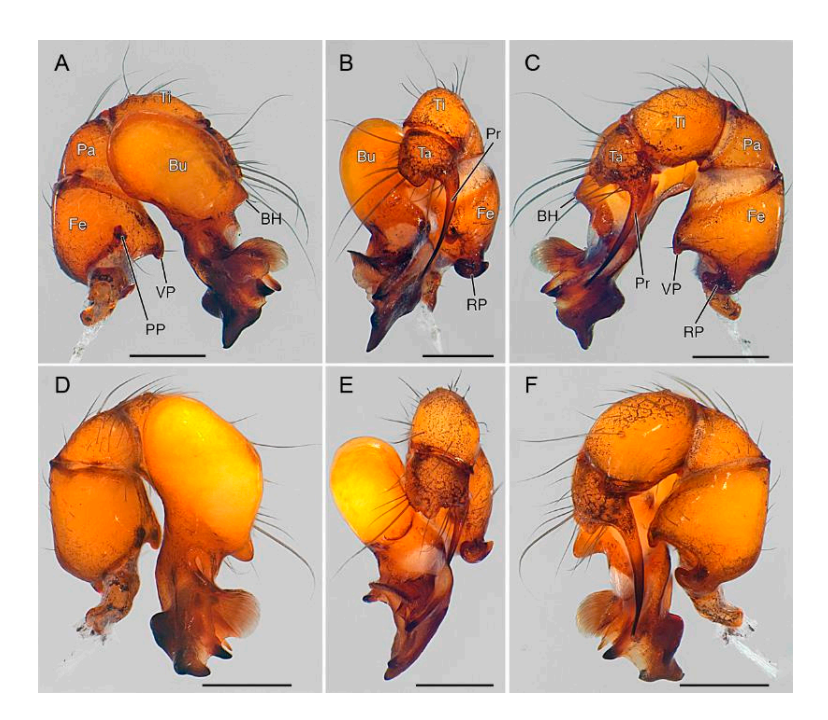


Figure 8. *Smeringopina polychila* sp. nov., male palps. (**A–C**). Male holotype (**D–F**). Male paratype (RMCA_247642), mirrored views. (**A,D**). Palp, prolateral view. (**B,E**). Idem, frontal view. (**C,F**). Idem, retrolateral view. Abbreviations: BH = bulbus hump; Bu = bulbus; Fe = femur; Pa = patella; Pr = procursus; PP = prolateral process of palpal femur; RP = retro-basal process of palpal femur; Ta = tarsus; Ti = tibia; VP = ventral process of palpal femur. Scale bars = 0.2 mm.

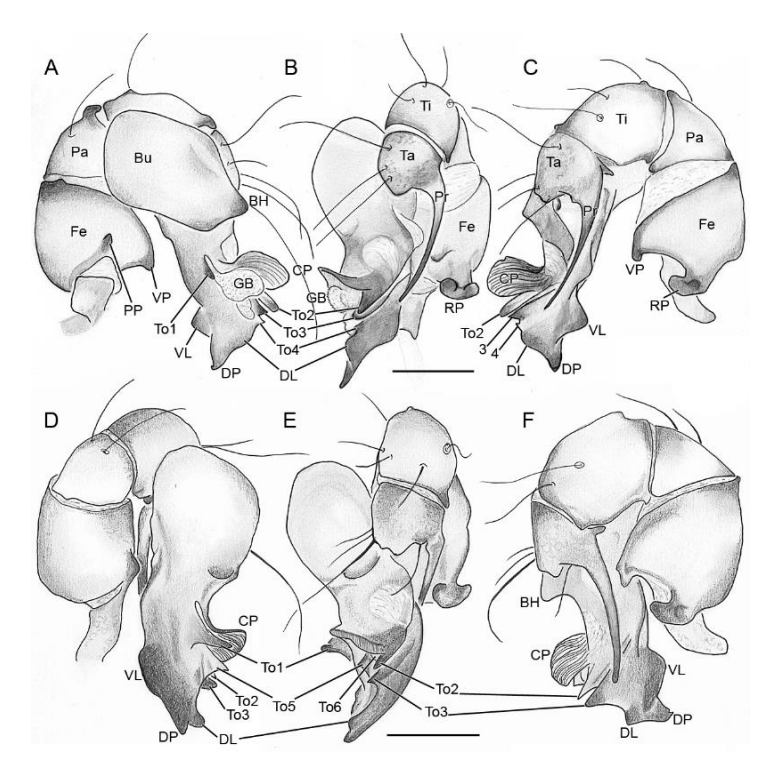


Figure 9. *Smeringopina polychila* sp. nov., genitalia drawings. (**A–C**) Male holotype. (**D–F**) Male paratype (RMCA_247642), mirrored views. (**A,D**) Palp, prolateral view. (**B,E**) Idem, frontal view. (**C,F**) Idem, retrolateral view. Abbreviations: BH = bulbus hump; Bu = bulbus; CP = cap-like plate; DL = dorsal lobe; DP = distal prong of bulbus; Fe = femur; GB = granulated bulge; Pa = patella; Pr = procursus; PP = prolateral process of palpal femur; RP = retro-basal process of palpal femur; Ta = tarsus; Ti = tibia; To1–6 = the different tooth-like appendages of bulbus; VL = ventral lobe; VP = ventral process of palpal femur. Scale bars = 0.2 mm.

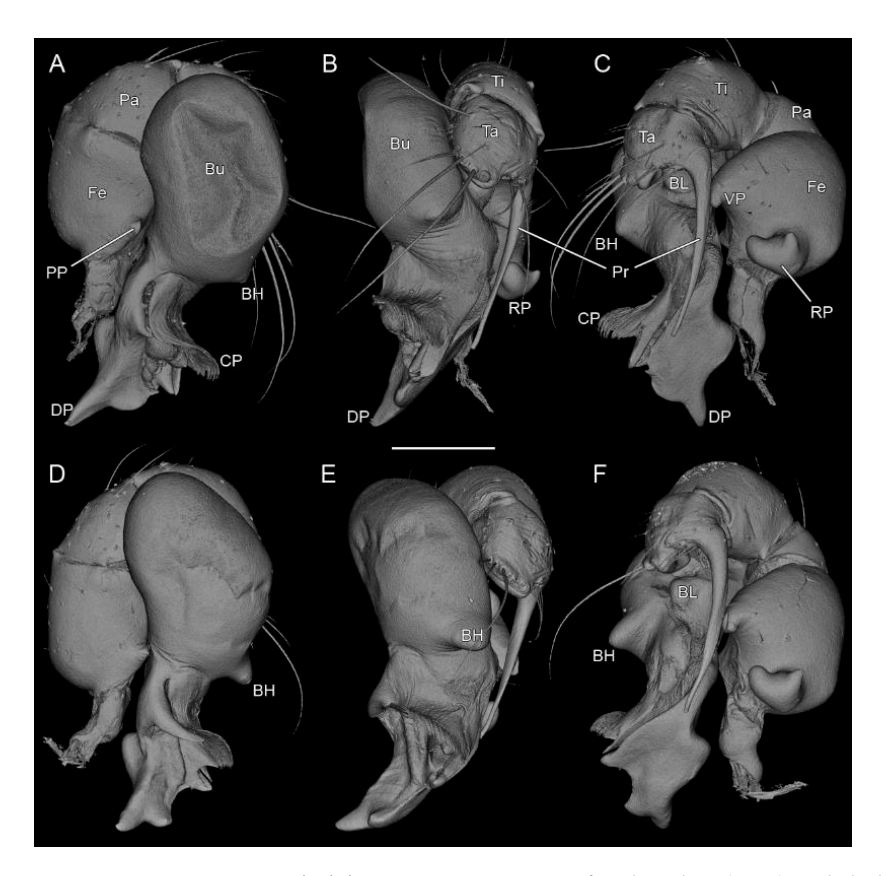


Figure 10. *Smeringopina polychila* sp. nov., μ CT scans of male palps. (**A–C**) Male holotype. (**D–F**) Male paratype (RMCA_247642), mirrored views. (**A,D**) Palp, prolateral view. (**B,E**) Idem, frontal view. (**C,F**) Idem, retrolateral view. Abbreviations: BH = bulbus hump; BL = prolateral bulbus lobe; Bu = bulbus; CP = cap-like plate; DP = distal prong of bulbus; Fe = femur; Pa = patella; Pr = procursus; PP = prolateral process of palpal femur; RP = retro-basal process of palpal femur; Ta = tarsus; Ti = tibia; VP = ventral process of palpal femur. Scale bars = 0.2 mm.

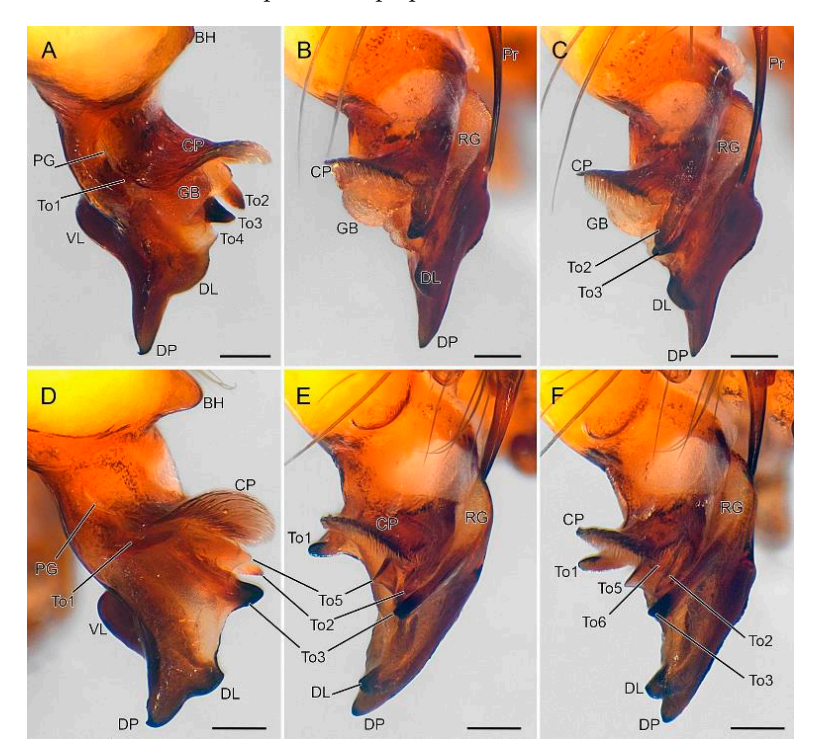


Figure 11. *Smeringopina polychila* sp. nov., detail of male palps (**A–C**) Male holotype. (**D–F**) Male paratype (RMCA_247642), mirrored views. (**A,D**) Apical part of palp, prolateral view. (**B,E**) Idem,

frontal view. (C,F) Idem, slightly retrolateral view. Abbreviations: BH = bulbus hump; CP = cap-like plate; DL = dorsal lobe; DP = distal prong of bulbus; GB = granulated bulge; PG = prolateral groove; Pr = procursus; RG: retrolateral groove; Pr = procursus; RG: retrolateral groove; Pr = procursus; RG: retrolateral groove; Pr = procursus; P

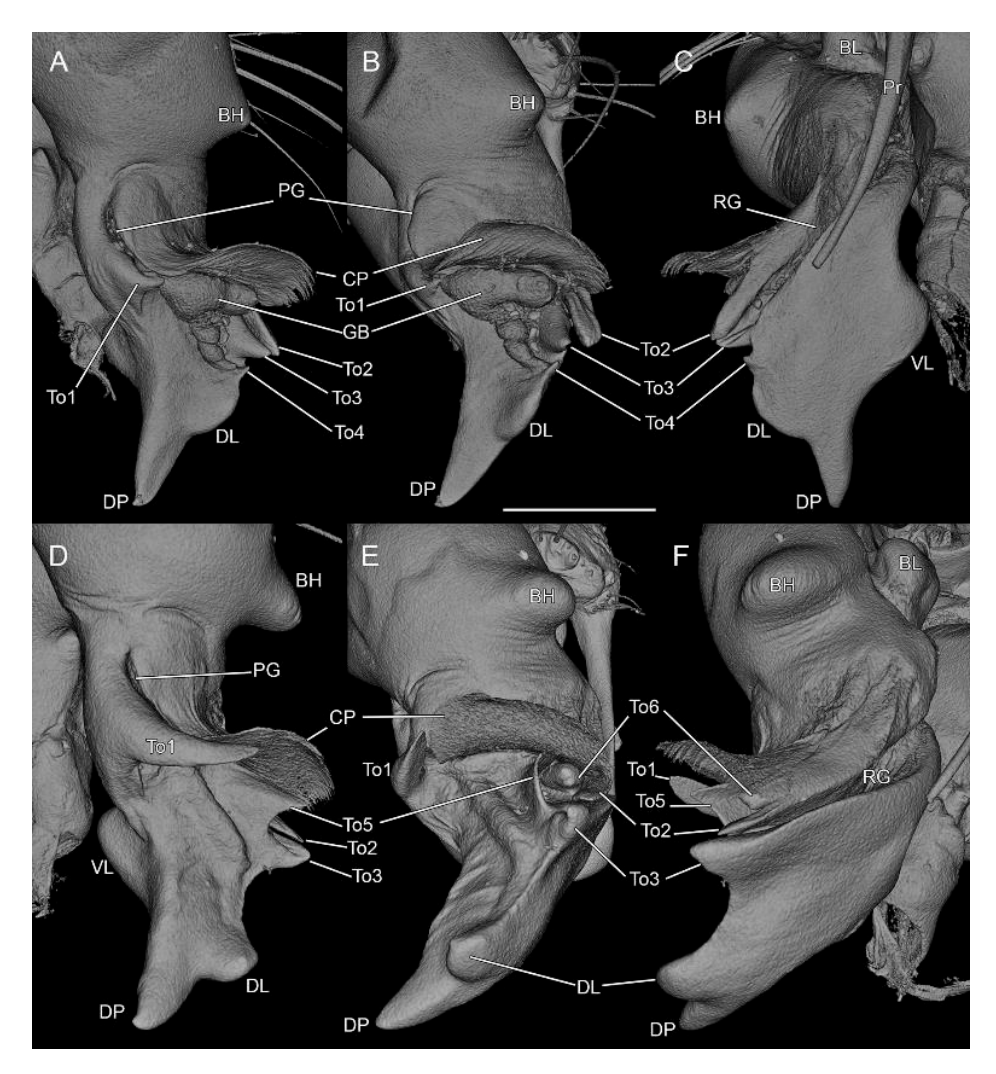


Figure 12. Smeringopina polychila sp. nov., detail of male palps in μ CT scans. (A–C) Male holotype. (D–F) Male paratype (RMCA_247642), mirrored views. (A,D) Apical part of palp, prolateral view. (B,E) Idem, frontal view. (C,F) Idem, retrolateral view. Abbreviations: BH = bulbus hump; BL = prolateral bulbus lobe; CP = cap-like plate; DL = dorsal lobe; DP = distal prong of bulbus; GB = granulated bulge; Pa = patella; PG = prolateral groove; Pr = procursus; RG: retrolateral groove; To1–6 = the different tooth-like appendages of bulbus; VL = ventral lobe. Scale bar = 0.5 mm.

Type material

Holotype

DR CONGO • ♂; Mai Ndombe Province, Malebo, Bopambu Forest, part of Nkombo Forest; 356 m asl; −2.43763, 16.63943; 21 October 2021; leg. M. Jocque; Winkler extraction of forest litter, riparian forest; BINCO_DRC_21_0001; RMCA_247638.

Paratypes

DR CONGO • 1 $\$; Same data as holotype; PQ349817 (COI); PQ350127 (16S); PQ356605 (H3); RMCA_247639 • 1 $\$; as previous; RMCA_247641 • 1 $\$; same data as previous; RMCA_247642 • 2 $\$ 3 subadults; collected by hand; further as holotype; PQ349818 (COI); PQ350128 (16S); PQ356606 (H3); RMCA_247640.



Figure 13. *Smeringopina polychila* sp. nov., female paratype (RMCA_247641). (**A**) Habitus, dorsal view. (**B**) Idem, ventral view. (**C**) Habitus, lateral view. (**D**) Abdomen, dorsal view. (**E**) Carapace, frontal view. (**F**) Idem, ventral view. Scale bars = (**A**–**D**) = 1 mm; (**E**,**F**) = 0.5 mm.

Etymology

The species name, *polychila*, is a noun in apposition referring to the presence of a chilum and two sclerites we call 'parachila' considering their position, so there are several 'chila'; hence, poly = many and chila.

Diagnosis

The male is easily recognized from all other Pholcidae by the presence of a large rectangular chilum (Chi) and two huge, ramified 'parachila' (Pch) as well as by the elevated shape of the carapace provided with lateral extensions (CAE) accommodated in the anterolateral concavities of the sternum (Figures 5 and 6). The female is unmistakable by its huge epigyne with very large, bulging anterior subcircular plate (AEP) provided with short tongue-shaped posterior protrusion (Figures 13C, 14 and 15).

Remark: to the best of our knowledge, these are so far the only known Pholcidae provided with a chilum and two large sclerites we here define as 'parachila'. Although the position of the single medial sclerite is typical for a chilum, we do not claim that it is homologous with that sclerite in, for instance, members of the RTA clade.

Description

Male (holotype RMCA_247638)

Measurements: total length 4.12; carapace width 1.49, length 1.85, height 1.21. Clypeus high 0.62. Sternum as long as wide 1.00. Eyes: AME 0.07; ALE 0.10; PME 0.12; PLE 2.11;

AME-AME 0.05; ALE-PLE touching; PME-PME 0.39; PME-ALE 0.15. Leg 1: 37.47 (10.15 + 0.50 + 9.59 + 15.95 + 1.28); tibia II 5.54; tibia III 4.62; tibia IV lost. leg I tibia length/diameter = 80.

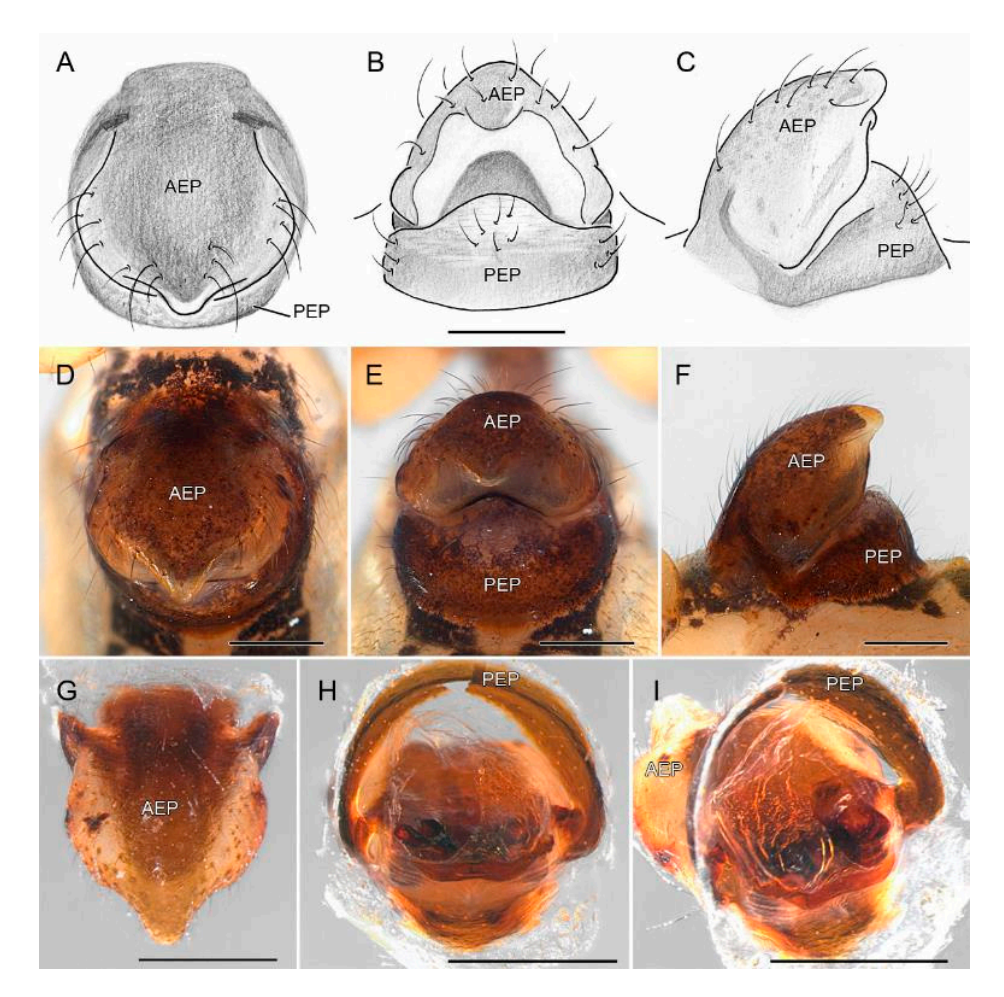


Figure 14. *Smeringopina polychila* sp. nov., female paratype (RMCA_247641) genitalia. (**A,D**) Epigyne, ventral view. (**B,E**) Idem, postero-ventral view. (**C,F**) Idem, lateral view. (**G**) Dissected epigyne, ventral view. (**H**) Endogyne, dorsal view. (**I**) Idem, slightly lateral view. Abbreviations: AEP = anterior epigynal plate; PEP = posterior epigynal plate. Scale bars = 0.5 mm.

Color in ethanol (Figures 4 and 5): carapace cephalic part orange, darkened around eyes and with black network dorsally and around eyes, darkened towards clypeus distal rim to brown-reddish above parachila; thoracic part yellow with dark triangle behind fovea and dark margins; thoracic and cephalic furrows darkened; chelicerae and labium dark brown, endites dark brown with two paler oval areas basally; sternum orange-brown densely mottled with black; chilum orange with darker stripe at base, parachila with dark brown base and dark orange appendages; abdomen uniform pale grey, darkened towards posterior tip.

Body: habitus as in Figures 4–7. Carapace with cephalic part strongly elevated, medially with faint furrow and ventrally with antero-lateral extensions (CAE), well delimited from thoracic part; both parts with shallow furrow converging towards deep oval-shaped fovea, posterior margin medially concave; chilum (Chi) subrectangular; parachila (Pch) with frontal, strongly developed semicircular excrescence at base and two ramified prongs, one originating halfway the length and provided with four or five large teeth, the second at the tip, with seven or eight teeth and provided with six or seven setae on retrolateral face (Figures 6C–E and 7A–F); clypeus strongly extended, approximately five times AME diameter, strongly sclerotized at level of each parachilum.

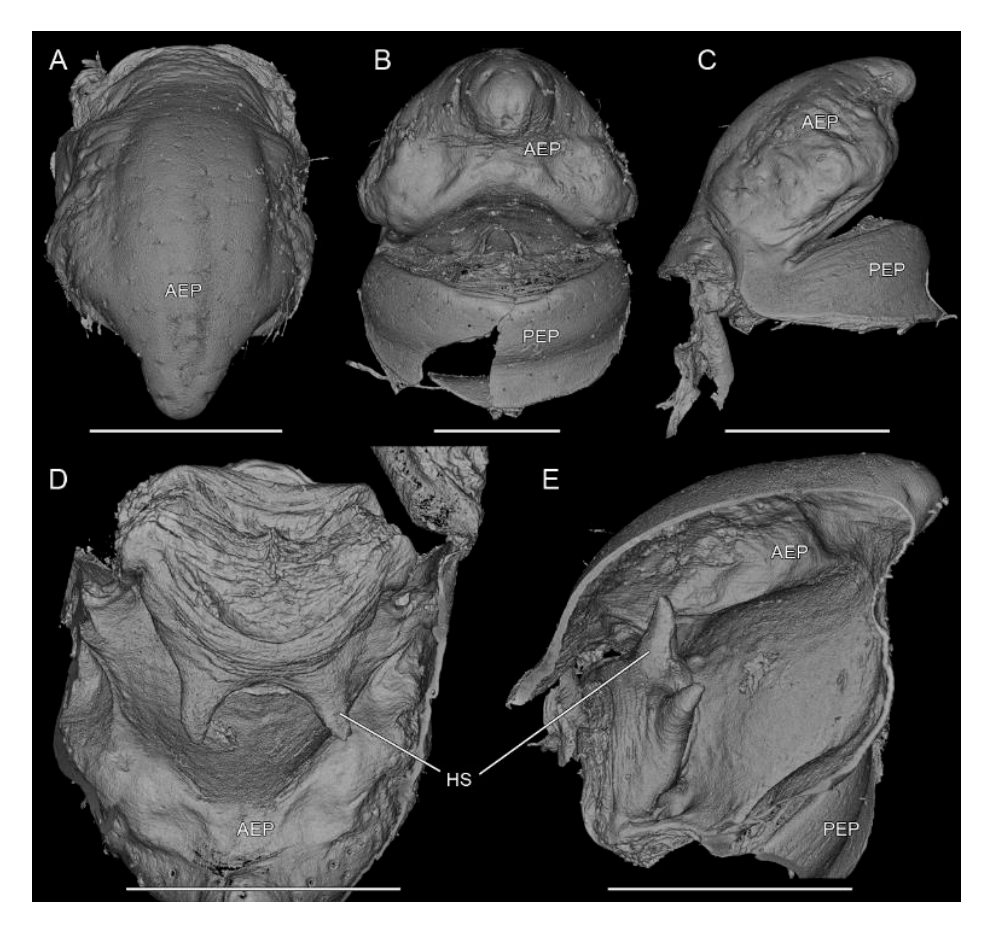


Figure 15. *Smeringopina polychila* sp. nov., female paratype (RMCA_247641) detail of genitalia in μ CT scans. (**A**) Epigyne, ventral view. (**B**) Idem, postero-ventral view. (**C**) Idem, lateral view. (**D**) Endogyne, dorsal view. (**E**) Endogyne, lateral view. Abbreviations: AEP = anterior epigynal plate; PEP = posterior epigynal plate; HS = horn-like internal structures. Scale bars = 0.5 mm.



Figure 16. Distribution of *Smeringopina polychila* sp. nov. in Africa (red dot). The map was created with the online tool SimpleMappr [22].

Sternum (Figure 5C,D) cup-shaped, frontal margin tightly close to base of labium, and deeply incurved on either side (SI) at endites level, delimiting membranous area accommodating extensions of cephalic part of carapace (CAE); posterior half with median, triangular depression.

Chelicerae (Che) unmodified (Figures 4B, 5D, 6C–E and 7A,D). Labium semicircular. Endites (En) with stout base and long, slightly flattened cylindrical apical extension; serrula present, single row.

Legs: finely haired, tarsal pseudo-segmentation invisible with dissecting microscope. Abdomen. Cylindrical–oval (Figure 4A. Remark: tegument torn and interior content lost). Palps: as in Figures 8–12; endite unmodified, trochanter tubular, slightly curved; femur (Fe) with one stout, bifid retro-basal process (RP), one recurved ventral process (VP), one small sub-basal prolateral process (PP); patella (Pa) unmodified; tibia (Ti) unmodified; tarsus (Ta) with rectangular sclerotized lip provided with five long curved setae and with simple, slender and pointed procursus (Pr) retrolaterally; bulbus (Bu) oval, with large prolateral rounded lobe (BL), small medial hump (BH) and several distal appendages: basal striated cap-like plate (CP) accompanied with median granulated bulge (GB) and lateral grooves; prolateral groove (PG) with inferior margin ending in stout tooth (To1); retrolateral groove (RG) accommodating procursus and with each margin ending in sharp tooth (To2 & To3); To3 grooved (Figure 12C–E); distal prong (DP) slightly curved, tapered, with dorsal (DL) and ventral lobes (VL); dorsal lobe with small basal triangular tooth (To4).

Remark: the opening of the sperm duct was not located. However, μ CT scans suggest it is situated at the groove present on To3 (see Appendix A.4).

Female (paratype RMCA_247641)

Similar to the male except for the ocular and clypeal areas.

Measurements: total length 3.76; carapace width 1.14, length 1.28, height 0.36. Eyes: AME 0.07; ALE 0.10; PME 0.10; PLE 0.12; AME-AME 0.05; ALE-PLE touching; PME-PME 0.18; PME-ALE 0.15. Leg 1: tibia 7.80; length/diameter = 97.

Color in ethanol (Figure 10): carapace pale yellow, darkened around eyes, with broad dark central band and narrow dark lateral margins; clypeus with two broad curved dark bands; chelicerae pale brown, sternum uniform dark brown, legs pale grey, femur, patella and tibia with darker stretches near joints; abdomen dorsum with faint dark pattern; venter with two medio-lateral dark spots just behind epigyne, each with two transverse pale stripes.

Body (Figure 13): carapace flat with deep, well-defined foveal pit; without anterolateral extensions; parachila absent; clypeus high, between 3.5 and 4 times AME diameter, anterior margin smoothly pointed. Sternum with antero-lateral margin deeply incurved, accommodating base of endites, without membranous area. Abdomen cylindrical. Legs: trochanters I reduced.

Epigyne (Figures 14 and 15): anterior epigynal plate (AEP) a large, strongly bulging capsule, almost as high as abdomen width, posterior margin slightly concave, distal tip with tongue-shaped protrusion pointing backward; posterior epigynal plate (PEP) well developed, subcircular; epigastric slit between AEP and PEP; AEP internally with two large hornlike structures (HS) (Figure 15D–E).

Variation

In male: The abdomen of the holotype is damaged and appears very different from the male paratype, which has a cylindrical shape (vs. oval) and both dorsum and venter are provided with a clear contrasting black and white pattern (Figure 4A vs. Figure 4C–E). Trochanters III are reduced in the paratype, presumably as a result of leg loss. The parachila of the paratype are slightly different from those in the holotype: in the shape and in the number of teeth (Figure 7A–D vs. Figure 7E,F). It is worth noting that in both specimens there is no perfect symmetry of the parachila. The palps of both individuals also present some remarkable differences: the male paratype has a palp with a more pronounced medial hump (BH) on the bulbus than the holotype (Figure 12A–C vs. Figure 12D–F); the prolateral tooth (To1) is much longer; the dorsal lobe (DL) of the distal prong is more strongly protruding and lacks the small tooth (To4) (Figures 9A–C and 12A–C vs. Figures 9D,E and

12D,E); the groove on To3 appears prolaterally whereas it is visible retrolaterally in the holotype (Figure 12C vs. Figure 12D,E); and the median granulated bulge (GB), present in both palps of the holotype, appears absent and this area is provided with one triangular and one conical structure (To5 & To6) (Figures 11A–C and 12A–C vs. Figures 11D–F and 12D–F). Remark: it might be that the granulated bulge in the holotype is a gelled exudate that probably hides those structures visible on the paratype. However, nothing could be seen even through μ CT scans.

It is also interesting to note that the subadult males, showing inflated palps, does not present any modification at the carapace and the chilum area, and thus lack the parachila. These structures apparently appear during the last molt.

Distribution

The species is only known from the type locality in north-western DR Congo (Figure 16).

4. Discussion

4.1. Phylogenetic Position of Smeringopina polychila sp. nov.

The genus Smeringopina was established by Kraus in 1957 [48] to accommodate several African representatives of Pholcidae. The genus received relatively little attention until the large-scale revision of West and Central African representatives by B. A. Huber in 2013 [8]. These revisions clarified species boundaries and substantially increased the number of recognized species to 44 species. Although the molecular analysis clearly shows that the new species described here is nested in Smeringopina, it is not clear in what species group it belongs. Huber [8] recognizes nine species groups but does not place S. ngungu Huber, 2013 because of its "aberrant" characters and therefore considers it incertae sedis. About the species described here, Huber (pers. comm. in litteris) wrote the following: "I have never seen something similar, I suspect it could be close to Smeringopina ngungu, also from DR Congo". Unfortunately, that species could not be sequenced and was not present in Huber et al.'s [14] molecular analysis of the family. From a morphological point of view, S. polychila sp. nov. shares some similarities with the representatives of the lekoni group like the abdominal pattern with a conspicuous lateral constriction of the dark ventral bands (char. 10 in [8]), and the palpal femur with stout basal apophyses (char. 35 in [8]). However, the new species lacks some diagnostic features defining the lekoni group: the chelicerae are unmodified, thus without apophyses (char. 18 in [8]), the palpal coxa is unmodified and thus not provided with a retrolateral apophysis (char. 30 in [8]); and the posterior epigynal plate is not laterally folded backwards to produce an overhang (char. 61 in [8]). As in Huber et al. [14], we did not recover the *lekoni* as group monophyletic (Figure 3). Therefore, in the present situation we have refrained from creating a new genus but also prefer not to place it in one of the species groups that have been recognized so far.

4.2. Sexual Characters and Variations

In our study, the use of micro-computed tomography (μ CT) proved particularly valuable for visualizing and interpreting intricate semi-translucent structures of the male palp, which are often difficult to distinguish with conventional 2D methods. The μ CT images and resulting 3D models also allowed us to better understand, and in some cases confirm, the morphological differences observed in the palps of the two males analysed. Furthermore, μ CT provided access to the internal organization of the female genitalia, such as the anterior plate of the epigyne, thereby revealing the shape and arrangement of internal structures. Together, these insights improved our morphological interpretation and underscore the potential of μ CT as a complementary tool in spider taxonomy.

The new species shows a strong sexual dimorphism, which is not uncommon among Pholcidae [49]. Modified structures of the male occurring on the chelicerae and the clypeus

enable the male to lock with the female for copulation [3,50–54]. In *Smeringopina*, males are provided with several apophyses on the chelicerae and the clypeus [8]. *S. polychila* sp. nov. is the first species of the genus without any apophyses on the chelicerae but instead bear remarkable parachilum structures. The parachila of the new species described here appear mobile, considering the different positions in the two males and the numerous muscular fibers visible with the μ CT scans (Figure 6C,E). We assume that, given the absence of cheliceral apophyses, these structures play a crucial role during mating, similarly enabling the male to position itself correctly relative to the female for copulation.

Interestingly, some morphological variations were observed between the two males analysed in this study. Unfortunately, our attempts to get DNA from both mature male specimens were unsuccessful. Intra-specific genital variation was already reported in some pholcid species [55,56], notably in Smeringopina (e.g., S. fang, S. moudouma or S. ebolowa, see [8]), but in these cases the males came from different populations. Proven intraspecific variation within one locality is extremely rare (e.g., [6]). Although the males here described show remarkable genitalic and somatic differences, we tentatively consider them conspecific. One of the main reasons is that, in both the holotype and the paratype, the left and right parachila differ in the number and arrangement of teeth at the extremity, clearly visible in Figure 7E. We assume that the secondary sexual characters of the males are so complex that there is some space for variation between right and left sides in a single specimen and certainly between different specimens. The fact that the parachila are movable may imply that their function is independent from the precise shape of the teeth. However, in cases where species limits may prove problematic like here, future in-depth research, involving additional specimens, localities, and genetic data, is required to test taxonomic conclusions. It should be questioned whether the rule for precision of morphology of copulatory organs and secondary sexual organs [57,58] may be stressed to a certain extent if these structures are very complex, in other words, whether 'precision is lost with complexity'. Our search for studies in this context did not yield any results and revealed that this field of research is untouched.

Author Contributions: Conceptualization, A.H. and R.J.; methodology—imaging and description, A.H. and R.J.; methodology—drawings, V.G.; methodology—µCT scans acquisition and curation, A.H.; methodology—DNA extraction, amplification and sequencing, N.S.; data curation, A.H. and N.S.; formal analysis, A.H. and N.S.; investigation, A.H., R.J. and N.S.; project administration, A.H. and R.J.; resources, A.H., R.J., N.S. and V.G.; writing—original draft preparation, A.H. and R.J.; writing—review and editing, A.H., R.J. and N.S.; visualization, A.H., R.J. and V.G.; validation, A.H. All authors have read and agreed to the published version of the manuscript.

Funding: The study was partially supported by the DiSSCo Fed program (Federal Support to the Distributed System of Scientific Collections, Contract FRSI/00/DI1) and by the Barcoding Facility for Organisms and Tissues of Policy Concern (BopCo—https://www.bopco.be/), both financed by the Belgian Science Policy Office (BELSPO).

Data Availability Statement: The original contributions presented in this study are included in the article. Further inquiries can be directed to the corresponding authors.

Acknowledgments: Merlijn Jocque is especially thanked for having collected, with the support of the organization Biodiversity Inventory for Conservation (BINCO) NPO, the specimens deposited at RMCA. We are grateful to Jonas Eberle, who kindly shared a .csv version of Table S1 from his previous work [2], facilitating the selection of taxa and sequences that were included in the present study. We thank Bernhard A. Huber for sharing his initial perspectives on this species and, together with two anonymous reviewers, for providing constructive comments that significantly improved the manuscript.

Conflicts of Interest: The authors declare no conflicts of interest. The funders had no role in the design of the study; in the collection, analyses, or interpretation of data; in the writing of the manuscript; or in the decision to publish the results.

Appendix A

Appendix A.1

Table A1. Primers involved in the amplification of the three selected DNA fragments.

Primer Name	Oligonucleotides	Reference	Target Region
C1-J-1718-spider C1-N-2776-spider	5'-GGNGGATTTGGAAATTGRTTRGTTCC-3' 5'-GGATAATCAGAATANCGNCGAGG-3'	[22] Vink et al. (2005)	Mitochondrial COI
LR-N-13398 (16Sar) LR-J-12887 (16Sbr)	5'-CGCCTGTTTAACAAAAACAT-3' 5'-CCGGTCTGAACTCAGATCACGT-3'	[23] Simon et al. (1994)	Mitochondrial 16S rRNA
H3aF H3aR	5'-ATGGCTCGTACCAAGCAGACVGC-3' 5'-ATATCCTTRGGCATRATRGTGAC-3'	[24] Colgan et al. (1998)	Nuclear histone H3

Appendix A.2

Table A2. PCR cycling conditions used for the amplification of the three selected DNA fragments.

Target Region	Initial Denaturation	Denaturation	Annealing	Elongation	Final Elongation	# of Cycles
COI	95 °C—15 min	94 °C—30 s	57 °C—90 s	72 °C—90 s	72 °C—10 min	45
16S	95 °C—15 min	94 °C—45 s 94 °C—45 s	45 °C—45 s 48 °C—45 s	72 °C—60 s 72 °C—60 s	72 °C—10 min	5 30
Н3	95 °C—15 min	94 °C—40 s	54 °C—50 s	72 °C—60 s	72 °C—10 min	40

Appendix A.3

Table A3. Smeringopinae sequences from GenBank analysed in this study. **Light shading:** sequences used in Dataset 1 (minimum two DNA fragments; Dataset 1 also includes Dataset 2 sequences). **Dark shading:** sequences included in Dataset 2 (minimum four DNA fragments). **Blue highlight:** sequences in Dataset 3 (*Smeringopina* only (regardless of the number of available genes), excluding *Smeringopus lesserti* and *S. lotzi*, both used as outgroups). **Bold:** representatives of the new species sequenced during this study (included in all Datasets). **Boxed:** sequences used to construct chimeric taxa.

C . 1.	Species -	Genetic Markers						Reference(s)
Code	Species -	12S	16S	18S	28S	COI	Н3	Reference(s)
RMCA_247639	Smeringopina polychila sp. nov.		PQ350127			PQ349817	PQ356605	Present study
RMCA_247640	Smeringopina polychila sp. nov.		PQ350128			PQ349818	PQ356606	Present study
M089	Cenemus culiculus				ON509570	ON504299	ON497107	[29] Huber & Meng 2023
BB05	Crossopriza lyoni	AY560689				AY560774		[26] Bruvo-Mađarić et al., 2005
Is2	Crossopriza lyoni	AY560690				AY560775		[26] Bruvo-Mađarić et al., 2005
P0154	Crossopriza lyoni	JX023767	JX023860	JX023957	JX024070	JX023551	JX023619	[2] Eberle et al., 2018; [14] Huber et al., 2018
SB026	Crossopriza lyoni	MG267734				MG268895		[2] Eberle et al., 2018; [14] Huber et al., 2018
S499	Crossopriza kittan	MG267718	MG268017	MG268336	MG268599	MG268821	MG269116	[2] Eberle et al., 2018; [14] Huber et al., 2018; [29] Huber & Meng 2023
S500	Crossopriza miskin	MG267719	MG268007	MG268337	MG268600	MG268820	MG269115	[2] Eberle et al., 2018; [14] Huber et al., 2018; [29] Huber & Meng 2023
S290	Crossopriza pristina	MG267546	MG267826	MG268155	MG268469	MG268894		[2] Eberle et al., 2018; [14] Huber et al., 2018
S435	Holocnemus reini	MG267665	MG267951	MG268277	MG268590	MG268890	MG269111	[2] Eberle et al., 2018; [14] Huber et al., 2018; [29] Huber & Meng 2023
P0233	Holocnemus hispanicus			JX024020		JX023600	JX023680	[2] Eberle et al., 2018; [14] Huber et al., 2018
BB06	Holocnemus pluchei	AY560691				AY560776		[26] Bruvo-Mađarić et al., 2005
HpIs2	Holocnemus pluchei	AY560692				AY560777		[26] Bruvo-Mađarić et al., 2005

Table A3. Cont.

	Cmasics			Professional (a)				
Code	Species –	12S	16S	18S	28S	COI	Н3	- Reference(s)
ZFMK	Holocnemus pluchei	JX023832		JX024036	JX024132		JX023687	[27] Dimitrov et al., 2013
ARASP087	Holocnemus pluchei	KY015507		KY016611	KY017265	KY017849		[28] Wheeler et al., 2017
S436	Hoplopholcus asiaeminoris	MG267666	MG267952	MG268278		MG268813		[2] Eberle et al., 2018; [14] Huber et al., 2018
S009	Hoplopholcus cecconii	MG267447		MG268084		MG268811		[2] Eberle et al., 2018; [14] Huber et al., 2018
S438	Hoplopholcus dim	MG267668	MG267954	MG268280		MG268815		[2] Eberle et al., 2018; [14] Huber et al., 2018; [16] Huber 2020
S057	Hoplopholcus forskali	MG267446	MG267758	MG268083				[2] Eberle et al., 2018; [14] Huber et al., 2018
S437	Hoplopholcus gazipasa	MG267667	MG267953	MG268279		MG268814		[2] Eberle et al., 2018; [14] Huber et al., 2018; [16] Huber 2020
S442	Hoplopholcus konya	MG267671	MG267958	MG268284	MG268558	MG268810		[2] Eberle et al., 2018; [14] Huber et al., 2018; [16] Huber 2020
S316	Hoplopholcus labyrinthi	MG267560	MG267849	MG268172		MG268808		[2] Eberle et al., 2018; [14] Huber et al., 2018
S315	Hoplopholcus minotaurinus	MG267559	MG267848	MG268171				[2] Eberle et al., 2018; [14] Huber et al., 2018
S314	Hoplopholcus minous	MG267558	MG267847	MG268170				[2] Eberle et al., 2018; [14] Huber et al., 2018
S439	Hoplopholcus patrizii		MG267955	MG268281		MG268807		[2] Eberle et al., 2018; [14] Huber et al., 2018
S440	Hoplopholcus sp. Tur21	MG267669	MG267956	MG268282		MG268812		[2] Eberle et al., 2018; [14] Huber et al., 2018
S441	Hoplopholcus suluin	MG267670	MG267957	MG268283		MG268809	MG269183	[2] Eberle et al., 2018; [14] Huber et al., 2018; [16] Huber 2020
CDE1 COE1	Smeringopina ankasa—GB51					MG268634		[2] Eberle et al., 2018; [14] Huber et al., 2018
GB51—S054	Smeringopina ankasa—S054		MG267772	MG268081				[2] Eberle et al., 2018; [14] Huber et al., 2018

Table A3. Cont.

	Species -			P ((2)				
Code	Species -	12S	16S	18S	28S	COI	Н3	Reference(s)
P0173	Smeringopina attuleh		JX023874				JX023633	[2] Eberle et al., 2018; [14] Huber et al., 2018
S491	Smeringopina bamenda	MG267710	MG267997				MG269120	[2] Eberle et al., 2018; [14] Huber et al., 2018
GB14	Smeringopina bayaka					MG268662		[2] Eberle et al., 2018; [14] Huber et al., 2018
GB15	Smeringopina belinga					MG268665		[2] Eberle et al., 2018; [14] Huber et al., 2018
P0152	Smeringopina bineti	JX023765	JX023858				JX023617	[2] Eberle et al., 2018; [14] Huber et al., 2018
S300	Smeringopina bomfobiri	MG267554	MG267834	MG268163		MG268633	MG269118	[2] Eberle et al., 2018; [14] Huber et al., 2018
S492	Smeringopina bwiti	MG267711	MG267998			MG268659	MG269068	[2] Eberle et al., 2018; [14] Huber et al., 2018
S042	Smeringopina camerunensis		MG267773	MG268079				[2] Eberle et al., 2018; [14] Huber et al., 2018
GB16	Smeringopina chaillu					MG268663		[2] Eberle et al., 2018; [14] Huber et al., 2018
S404	Smeringopina djidji	MG267602	MG267930	MG268220		MG268666	MG269069	[2] Eberle et al., 2018; [14] Huber et al., 2018
GB52—P0175	Smeringopina ebolowa—GB52					MG268668		[2] Eberle et al., 2018; [14] Huber et al., 2018
GB32—10173	Smeringopina ebolowa—P0175	JX023786	JX023876				JX023635	[2] Eberle et al., 2018; [14] Huber et al., 2018
GB17	Smeringopina essotah					MG268664		[2] Eberle et al., 2018; [14] Huber et al., 2018
GB18	Smeringopina fang					MG268654		[2] Eberle et al., 2018; [14] Huber et al., 2018
P0153	Smeringopina guineensis	JX023766	JX023859			JX023550	JX023618	[2] Eberle et al., 2018; [14] Huber et al., 2018

Table A3. Cont.

Code	Species -			Genetic	Markers			- Reference(s)
Code	Species -	12S	16S	18S	28S	COI	Н3	Ketetefice(s)
GB19	Smeringopina iboga					MG268645		[2] Eberle et al., 2018; [14] Huber et al., 2018
S041	Smeringopina kala	MG267459	MG267774	MG268078	MG268387	MG268622	MG269119	[2] Eberle et al., 2018; [14] Huber et al., 2018
S402	Smeringopina kinguele	MG267600	MG267928	MG268219	MG268527		MG269181	[2] Eberle et al., 2018; [14] Huber et al., 2018
S044	Smeringopina kribi	MG267460	MG267775	MG268080		MG268660		[2] Eberle et al., 2018; [14] Huber et al., 2018
GB20	Smeringopina lekoni					MG268652		[2] Eberle et al., 2018; [14] Huber et al., 2018
S043	Smeringopina mbouda		MG267776	MG268082			MG269066	[2] Eberle et al., 2018; [14] Huber et al., 2018
S403	Smeringopina mohoba	MG267601	MG267929			MG268655	MG269182	[2] Eberle et al., 2018; [14] Huber et al., 2018
S049	Smeringopina moudouma	MG267462	MG267777	MG268077	MG268386			[2] Eberle et al., 2018; [14] Huber et al., 2018
GB21	Smeringopina ndjole					MG268644		[2] Eberle et al., 2018; [14] Huber et al., 2018
P0180	Smeringopina nyasoso	JX023790	JX023880			JX023565	JX023639	[2] Eberle et al., 2018; [14] Huber et al., 2018
S405	Smeringopina ogooue	MG267603	MG267931			MG268669	MG269070	[2] Eberle et al., 2018; [14] Huber et al., 2018
GB22	Smeringopina sahoue					MG268658		[2] Eberle et al., 2018; [14] Huber et al., 2018
S493	Smeringopina simintang	MG267716	MG267999	MG268329		MG268667		[2] Eberle et al., 2018; [14] Huber et al., 2018
S301	Smeringopina tchimbele		MG267835	MG268164		MG268661	MG269067	[2] Eberle et al., 2018; [14] Huber et al., 2018

24 of 28

Table A3. Cont.

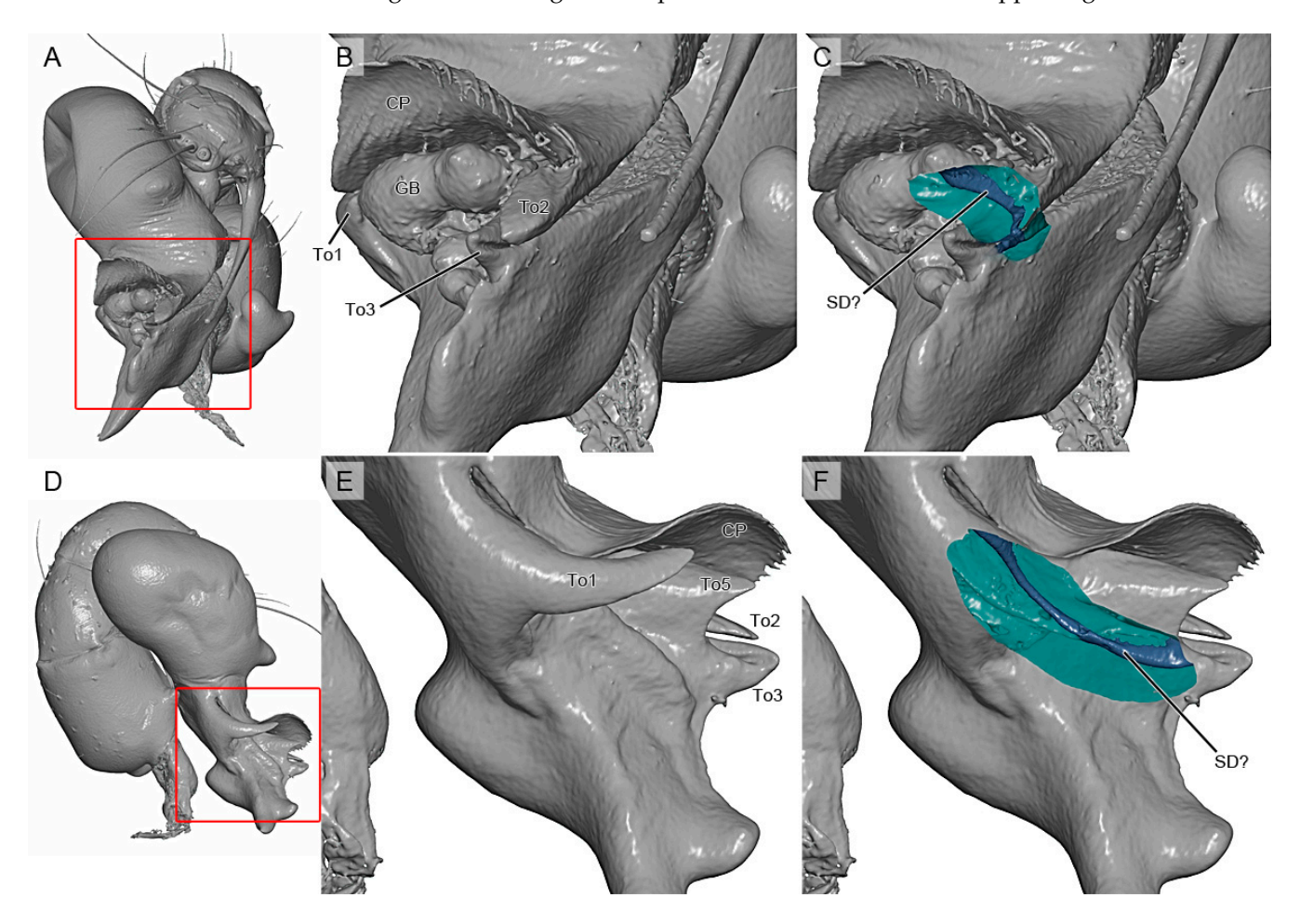
C. I.	Species -			Genetic	Markers			- Reference(s)
Code	Species -	12S	16S	18S	28S	COI	Н3	= Keterence(s)
GB54—S050	Smeringopina tebe—GB54					MG268653		[2] Eberle et al., 2018; [14] Huber et al., 2018
GD34—3030	Smeringopina tebe—\$050	MG267461	MG267778	MG268076				[2] Eberle et al., 2018; [14] Huber et al., 2018
S017	Smeringopus arambourgi	MG267458	MG267779	MG268039	MG268382		MG269061	[2] Eberle et al., 2018; [14] Huber et al., 2018
P0266	Smeringopus bujongolo	JX023837	JX023933	JX024045			JX023697	[2] Eberle et al., 2018; [14] Huber et al., 2018
P0224	Smeringopus cf. atomarius		JX023910	JX024012	JX024117		JX023673	[2] Eberle et al., 2018; [14] Huber et al., 2018
P0227	Smeringopus cf. similis	JX023820	JX023912	JX024015	JX024119		JX023675	[2] Eberle et al., 2018; [14] Huber et al., 2018
P0161	Smeringopus chogoria	JX023774	JX023866	JX023963		JX023555		[27] Dimitrov et al., 2013; [2] Eberle et al., 2018; [14] Huber et al., 2018
P0143	Smeringopus cylindrogaster		JX023850	JX023951	JX024064			[2] Eberle et al., 2018; [14] Huber et al., 2018
P0178	Smeringopus cylindrogaster		JX023878	JX023975	JX024084			[2] Eberle et al., 2018; [14] Huber et al., 2018
S407	Smeringopus lesserti	MG267605	MG267933	MG268222	MG268530	MG268871	MG269062	[2] Eberle et al., 2018; [14] Huber et al., 2018
S408	Smeringopus lotzi	MG267606	MG267934	MG268223	MG268529	MG268872	MG269063	[2] Eberle et al., 2018; [14] Huber et al., 2018
P0257	Smeringopus mgahinga		JX023927	JX024038			JX023688	[2] Eberle et al., 2018; [14] Huber et al., 2018
P0265	Smeringopus mpanga		JX023932				JX023696	[2] Eberle et al., 2018; [14] Huber et al., 2018
BB28	Smeringopus natalensis	AY560717			AY560755			[2] Eberle et al., 2018; [14] Huber et al., 2018
P0157	Smeringopus ngangao	JX023770	JX023863	JX023960	JX024073			[2] Eberle et al., 2018; [14] Huber et al., 2018

Table A3. Cont.

C. 1.	Species -			- Reference(s)				
Code	Species -	12S	16S	18S	28S	COI	Н3	Keterence(s)
P0264	Smeringopus pallidus	JX023836	JX023931	JX024044	JX024136		JX023695	[2] Eberle et al., 2018; [14] Huber et al., 2018
S406	Smeringopus peregrinoides	MG267604	MG267932	MG268221	MG268528		MG269060	[2] Eberle et al., 2018; [14] Huber et al., 2018
S108	Stygopholcus skotophilus	MG267487		MG268112	MG268428	MG268938		[2] Eberle et al., 2018; [14] Huber et al., 2018; [29] Huber & Meng 2023
S109	Stygopholcus montenegrinus	MG267488				MG268936		[2] Eberle et al., 2018; [14] Huber et al., 2018; [29] Huber & Meng 2023
S112	Stygopholcus skotophilus	MG267490		MG268114	MG268430	MG268937		[2] Eberle et al., 2018; [14] Huber et al., 2018; [29] Huber & Meng 2023
S317	Stygopholcus photophilus	MG267561	MG267850	MG268173		MG268934	MG269114	[2] Eberle et al., 2018; [14] Huber et al., 2018
S110	Stygopholcus absoloni	MG267489		MG268113	MG268429	MG268935		[2] Eberle et al., 2018; [14] Huber et al., 2018; [29] Huber & Meng 2023
P0164	Spermophora minotaura	JX023777	JX023869	JX023965	JX024077	JX023557	JX023624	[2] Eberle et al., 2018; [14] Huber et al., 2018

Appendix A.4

Graphic reconstructions of the male palps of *Smeringopina polychila* sp. nov., processed in GOM Inspect and edited in Photoshop CS5. The supposed sperm duct (SD) is shown converging toward bulbus appendage To3. Coloured areas represent the internal part of the bulbus. (A–C) Male holotype, frontal view (the red box indicates the region of the bulbus detailed in B & C); (D–E) Male paratype (RMCA_247642), prolateral view (the red box indicates the region of the bulbus detailed in E & F). Abbreviations: CP = cap-like plate; CP = cap-like plate



References

- 1. World Spider Catalog Version 26 (2025). Natural History Museum Bern. Available online: http://wsc.nmbe.ch (accessed on 1 June 2025). [CrossRef]
- 2. Eberle, J.; Dimitrov, D.; Valdez-Mondragón, A.; Huber, B.A. Microhabitat change drives diversification in pholcid spiders. *BMC Evol. Biol.* **2018**, *18*, 141. [CrossRef]
- 3. Huber, B.A. Sexual selection in pholcid spiders (Araneae, Pholcidae): Artful chelicerae and forceful genitalia. *J. Arachnol.* **1999**, 27, 135–141.
- 4. Huber, B.A. High species diversity, male-female coevolution, and metaphyly in Southeast Asian pholcid spiders: The case of *Belisana* Thorell 1898 (Araneae, Pholcidae). *Zoologica* **2005**, *155*, 1–126.
- 5. Huber, B.A. Two new genera of small, six-eyed pholcid spiders from West Africa, and first record of *Spermophorides* for mainland Africa (Araneae: Pholcidae). *Zootaxa* **2007**, *1635*, 23–43. [CrossRef]
- 6. Huber, B.A. Revision and cladistic analysis of *Pholcus* and closely related taxa (Araneae, Pholcidae). *Bonn. Zool. Monogr.* **2011**, *58*, 1–509.
- 7. Huber, B.A. Revision and cladistic analysis of the Afrotropical endemic genus *Smeringopus* Simon, 1890 (Araneae: Pholcidae). *Zootaxa* **2012**, *3461*, 1–138. [CrossRef]

Taxonomy **2025**, 5, 57 27 of 28

8. Huber, B.A. Revision and cladistic analysis of the Guineo-Congolian spider genus *Smeringopina* Kraus (Araneae, Pholcidae). *Zootaxa* **2013**, *3713*, 1–160. [CrossRef] [PubMed]

- 9. Huber, B.A. A new genus of ground and litter-dwelling pholcine spiders from Sarawak (Araneae, Pholcidae). *Eur. J. Taxon.* **2016**, 186, 1–15. [CrossRef]
- 10. Huber, B.A.; Nuñeza, O.M. Evolution of genital asymmetry, exaggerated eye stalks, and extreme palpal elongation in *Panjange* spiders (Araneae: Pholcidae). *Eur. J. Taxon.* **2015**, *169*, 1–46. [CrossRef]
- 11. Aharon, S.; Huber, B.A.; Gavish-Regev, E. Daddy-long-leg giants: Revision of the spider genus *Artema* Walckenaer, 1837 (Araneae, Pholcidae). *Eur. J. Taxon.* **2017**, *376*, 1–57. [CrossRef]
- 12. Huber, B.A.; Kwapong, P. West African pholcid spiders: An overview, with descriptions of five new species (Araneae, Pholcidae). *Eur. J. Taxon.* **2013**, *59*, 1–44. [CrossRef]
- 13. Huber, B.A.; Meng, G.L.; Král, J.; Ávila Herrera, I.M.; Carvalho, L.S. Diamonds in the rough: *Ibotyporanga* (Araneae, Pholcidae) spiders in semi-arid Neotropical environments. *Eur. J. Taxon.* **2024**, *963*, 1–169. [CrossRef]
- 14. Huber, B.A.; Eberle, J.; Dimitrov, D. The phylogeny of pholcid spiders: A critical evaluation of relationships suggested by molecular data (Araneae, Pholcidae). *ZooKeys* **2018**, *789*, 51–101. [CrossRef] [PubMed]
- 15. Huber, B.A.; Carvalho, L.S. Filling the gaps: Descriptions of unnamed species included in the latest molecular phylogeny of Pholcidae (Araneae). *Zootaxa* **2019**, 4546, 1–96. [CrossRef] [PubMed]
- 16. Huber, B.A. Revision of the spider genus Hoplopholcus Kulczyński (Araneae, Pholcidae). Zootaxa 2020, 4726, 1–94. [CrossRef]
- 17. Huber, B.A. Revisions of *Holocnemus* and *Crossopriza*: The spotted-leg clade of Smeringopinae (Araneae, Pholcidae). *Eur. J. Taxon.* **2022**, 795, 1–241. [CrossRef]
- 18. Huber, B.A. The South American spider genera *Mesabolivar* and *Carapoia* (Araneae, Pholcidae): New species and a framework for redrawing generic limits. *Zootaxa* **2018**, 4395, 1–178. [CrossRef]
- 19. Jocqué, R.; Jocque, M.; Mbende, M. A new *Cangoderces* (Araneae, Telemidae) from DR Congo, the first telemid from Central Africa. *Zootaxa* **2022**, 5162, 430–438. [CrossRef]
- 20. Jocqué, R. How to rehydrate dried spiders. Newsl. Br. Arachnol. Soc. 2008, 112, 5.
- 21. Beccaloni, J. A preliminary comparison of Trisodium Phosphate with Agepon and Decon90 as wetting agents to hydrate dried arachnida and myriapoda specimens. *NatSCA News* **2012**, *22*, 71–79.
- 22. SimpleMappr, an Online Tool to Produce Publication-Quality Point Maps. Shorthouse D.P. 2010. Available online: https://www.simplemappr.net (accessed on 1 January 2023).
- 23. Vink, C.J.; Thomas, S.M.; Paquin, P.; Hayashi, C.Y.; Hedin, M. The effects of preservatives and temperatures on arachnid DNA. *Invertebr. Syst.* **2005**, *19*, 99–104. [CrossRef]
- 24. Simon, C.; Frati, F.; Beckenbach, A.; Crespi, B.; Liu, H.; Flook, P. Evolution, Weighting, and Phylogenetic Utility of Mitochondrial Gene Sequences and a Compilation of Conserved Polymerase Chain Reaction Primers. *Ann. Entomol. Soc. Am.* 1994, 87, 651–701. [CrossRef]
- 25. Colgan, D.J.; McLauchlan, A.; Wilson, G.D.F.; Livingston, S.P.; Edgecombe, G.D.; Macaranas, J.; Cassis, G.; Gray, M.R. Histone H3 and U2 snRNA DNA sequences and arthropod molecular evolution. *Aust. J. Zool.* **1998**, *46*, 419–437. [CrossRef]
- 26. Ratnasingham, S.; Hebert, P.D.N. BOLD: The Barcode of Life Data System. Mol. Ecol. Notes 2007, 7, 355–364. [CrossRef] [PubMed]
- 27. Bruvo-Madarić, B.; Huber, B.A.; Steinacher, A.; Pass, G. Phylogeny of pholcid spiders (Araneae: Pholcidae): Combined analysis using morphology and molecules. *Mol. Phylogenetics Evol.* **2005**, *37*, 661–673. [CrossRef] [PubMed]
- 28. Dimitrov, D.; Astrin, J.J.; Huber, B.A. Pholcid spider molecular systematics revisited, with new insights into the biogeography and the evolution of the group. *Cladistics* **2013**, *29*, 132–146. [CrossRef]
- 29. Wheeler, W.C.; Coddington, J.A.; Crowley, L.M.; Dimitrov, D.; Goloboff, P.A.; Griswold, C.E.; Hormiga, G.; Prendini, L.; Ramírez, M.J.; Sierwald, P.; et al. The spider tree of life: Phylogeny of Araneae based on target-gene analyses from an extensive taxon sampling. *Cladistics* **2017**, *33*, 576–616. [CrossRef]
- Huber, B.A.; Meng, G.L. On the mysterious Seychellois endemic spider genus Cenemus (Araneae, Pholcidae). Arthropod Syst. Phylogeny 2023, 81, 179–200. [CrossRef]
- 31. Astrin, J.J.; Misof, B.; Huber, B.A. The pitfalls of exaggeration: Molecular and morphological evidence suggests *Kaliana* is a synonym of *Mesabolivar* (Araneae: Pholcidae). *Zootaxa* **2007**, *1646*, 17–30. [CrossRef]
- 32. Katoh, K.; Standley, D.M. MAFFT Multiple Sequence Alignment Software Version 7: Improvements in performance and usability. *Mol. Biol. Evol.* **2013**, *30*, 772–780. [CrossRef]
- 33. Castresana, J. Selection of conserved blocks from multiple alignments for their use in phylogenetic analysis. *Mol. Biol. Evol.* **2000**, 17, 540–552. [CrossRef] [PubMed]
- 34. Talavera, G.; Castresana, J. Improvement of phylogenies after removing divergent and ambiguously aligned blocks from protein sequence alignments. *Syst. Biol.* **2007**, *56*, 564–577. [CrossRef] [PubMed]

Taxonomy 2025, 5, 57 28 of 28

35. Dereeper, A.; Guignon, V.; Blanc, G.; Audic, S.; Buffet, S.; Chevenet, F.; Dufayard, J.F.; Guindon, S.; Lefort, V.; Lescot, M.; et al. Phylogeny.fr: Robust phylogenetic analysis for the non-specialist. *Nucleic Acids Res.* **2008**, *36* (Suppl. 2), W465–W469. [CrossRef] [PubMed]

- 36. Lemoine, F.; Correia, D.; Lefort, V.; Doppelt-Azeroual, O.; Mareuil, F.; Cohen-Boulakia, S.; Gascuel, O. NGPhylogeny.fr: New generation phylogenetic services for non-specialists. *Nucleic Acids Res.* **2019**, *47*, W260–W265. [CrossRef]
- 37. Mesquite: A Modular System for Evolutionary Analysis, Version 3.8, Maddison, W.P. and D.R. Maddison. 2023. Available online: http://www.mesquiteproject.org (accessed on 10 January 2024).
- 38. Lanfear, R.; Frandsen, P.B.; Wright, A.M.; Senfeld, T.; Calcott, B. PartitionFinder 2: New methods for selecting partitioned models of evolution for molecular and morphological phylogenetic analyses. *Mol. Biol. Evol.* **2016**, *34*, 772–773. [CrossRef]
- 39. Guindon, S.; Dufayard, J.F.; Lefort, V.; Anisimova, M.; Hordijk, W.; Gascuel, O. New algorithms and methods to estimate maximum-likelihood phylogenies: Assessing the performance of PhyML 3.0. *Syst. Biol.* **2010**, *59*, 307–321. [CrossRef]
- 40. Lanfear, R.; Calcott, B.; Ho, S.Y.; Guindon, S. PartitionFinder: Combined selection of partitioning schemes and substitution models for phylogenetic analyses. *Mol. Biol. Evol.* **2012**, *29*, 1695–1701. [CrossRef]
- 41. Zwickl, D.J. Genetic Algorithm Approaches for the Phylogenetic Analysis of Large Biological Sequence Datasets Under the Maximum Likelihood Criterion. Ph.D. Dissertation, The University of Texas, Austin, TX, USA, May 2006.
- 42. Sukumaran, J.; Holder, M.T. DendroPy: A Python library for phylogenetic computing. *Bioinformatics* **2010**, *26*, 1569–1571. [CrossRef]
- 43. Huelsenbeck, J.P.; Ronquist, F. MRBAYES: Bayesian inference of phylogeny. Bioinformatics 2001, 17, 754–755. [CrossRef]
- 44. Ronquist, F.; Huelsenbeck, J.P. MRBAYES 3: Bayesian phylogenetic inference under mixed models. *Bioinformatics* **2003**, *19*, 1572–1574. [CrossRef]
- 45. Ronquist, F.; Teslenko, M.; van der Mark, P.; Ayres, D.L.; Darling, A.; Höhna, S.; Larget, B.; Liu, L.; Suchard, M.A.; Huelsenbeck, J.P. MrBayes 3.2: Efficient Bayesian Phylogenetic Inference and Model Choice Across a Large Model Space. *Syst. Biol.* **2012**, *61*, 539–542. [CrossRef] [PubMed]
- 46. Rambaut, A.; Drummond, A.J.; Xie, D.; Baele, G.; Suchard, M.A. Posterior Summarization in Bayesian Phylogenetics Using Tracer 1.7. Syst. Biol. 2018, 67, 901–904. [CrossRef] [PubMed]
- 47. Figtree Version 1.4.4, Rambaut R. 2006–2018. Available online: http://tree.bio.ed.ac.uk/software/figtree/ (accessed on 9 January 2024).
- 48. Kraus, O. Araneenstudien 1. Pholcidae (Smeringopodinae, Ninetinae). Senckenberg. Biol. 1957, 38, 217–243.
- 49. Huber, B.A. Beyond size: Sexual dimorphisms in pholcid spiders. Arachnology 2021, 18, 656–677. [CrossRef]
- 50. Huber, B.A. Genital morphology, copulatory mechanism and reproductive biology in *Psilochorus simoni* (Berland, 1911) (Pholcidae; Araneae). *Neth. J. Zool.* **1994**, *44*, 85–99. [CrossRef]
- 51. Huber, B.A. Copulatory mechanism in *Holocnemus pluchei* and *Pholcus opilionoides*, with notes on male cheliceral apophyses and stridulatory organs in Pholcidae (Araneae). *Acta Zool.* **1995**, *76*, 291–300. [CrossRef]
- 52. Huber, B.A. On American 'Micromerys' and Metagonia (Araneae, Pholcidae), with notes on natural history and genital mechanics. Zool. Scr. 1997, 25, 341–363. [CrossRef]
- 53. Huber, B. Genital mechanics in some neotropical pholcid spiders (Araneae: Pholcidae), with implications for systematics. *J. Zool.* **1998**, 244, 587–599. [CrossRef]
- 54. Huber, B.A.; Eberhard, W.G. Courtship, copulation, and genital mechanics in *Physocyclus globosus* (Araneae, Pholcidae). *Can. J. Zool.* **1997**, 74, 905–918. [CrossRef]
- 55. Huber, B.A.; Pérez-González, A.; Astrin, J.J.; Blume, C.; Baptista, R. *Litoporus iguassuensis* Mello-Leitão, 1918 (Araneae, Pholcidae): Camouflaged retreat, sexual dimorphism, female color polymorphism, intra-specific genital variation, and description of the male. *Zool. Anz.* 2013, 252, 511–521. [CrossRef]
- 56. Huber, B.A.; Dimitrov, D. Slow genital and genetic but rapid non-genital and ecological differentiation in a pair of spider species (Araneae, Pholcidae). *Zool. Anz.* **2014**, 253, 394–403. [CrossRef]
- 57. Wheeler, Q.D.; Platnick, N. The phylogenetic species concept. In *Species Concepts and Phylogenetic Theory. A Debate*; Wheeler, Q.D., Meier, R., Eds.; Columbia University Press: New York, NY, USA, 2000; pp. 55–69.
- 58. Eberhard, W.G.; Huber, B.A.; Rodriguez, R.L.S.; Briceño, R.D.; Salas, I.; Rodriguez, V. One size fits all? Relationships between the size and degree of variation in genitalia and other body parts in twenty species of insects and spiders. *Evolution* **1998**, *52*, 415–431. [CrossRef]

Disclaimer/Publisher's Note: The statements, opinions and data contained in all publications are solely those of the individual author(s) and contributor(s) and not of MDPI and/or the editor(s). MDPI and/or the editor(s) disclaim responsibility for any injury to people or property resulting from any ideas, methods, instructions or products referred to in the content.